Cell count moments in the halo model

J. N. Fry,[1,2]★ S. Colombi,[2]★ Pablo Fosalba,[3]★ Anand Balaraman,[1,4]★ István Szapudi[5]★ and R. Teyssier[6,7]★

[1]*Department of Physics, University of Florida, Gainesville, FL 32611-8440, USA*
[2]*Institut d'Astrophysique de Paris & UPMC (UMR 7095), 98 bis boulevard Arago, 75014 Paris, France*
[3]*Institut de Ciències de l'Espai, IEEC–CSIC, Campus UAB, F. de Ciències, Torre C5 par-2, Barcelona 08193, Spain*
[4]*Department of Physics, Georgia Southern University, Statesboro, GA 30460, USA*
[5]*Institute for Astronomy, University of Hawaii, 2680 Woodlawn Drive, Honolulu, HI 96822, USA*
[6]*Service d'Astrophysique, CEA Saclay, Orme des Merisiers, 91191 Gif-sur-Yvette Cedex, France*
[7]*Institut für Theoretische Physik, Universität Zürich, Winterthurer Strasse 190, CH-8057 Zürich, Switzerland*

ABSTRACT

We study cell count moments up to fifth order of the distributions of haloes, of halo substructures as a proxy for galaxies, and of mass in the context of the halo model and compare theoretical predictions to the results of numerical simulations. On scales larger than the size of the largest cluster, we present a simple point cluster model in which results depend only on cluster–cluster correlations and on the distribution of the number of objects within a cluster, or cluster occupancy. The point cluster model leads to expressions for moments of galaxy counts in which the volume-averaged moments on large scales approach those of the halo distribution and on smaller scales exhibit hierarchical clustering with amplitudes S_k determined by moments of the occupancy distribution. In this limit, the halo model predictions are purely combinatoric, and have no dependence on halo profile, concentration parameter or potential asphericity. The full halo model introduces only two additional effects: on large scales, haloes of different mass have different clustering strengths, introducing relative bias parameters; and on the smallest scales, halo structure is resolved and details of the halo profile become important, introducing shape-dependent form factors. Because of differences between discrete and continuous statistics, the hierarchical amplitudes for galaxies and for mass behave differently on small scales even if galaxy number is exactly proportional to mass, a difference that is not necessarily well described in terms of bias.

Key words: methods: numerical – methods: statistical – large-scale structure of Universe.

1 INTRODUCTION

Describing the properties of the distribution of matter in the Universe in terms of the masses, spatial distribution and shapes of clusters, or haloes, is an enterprise with a long history (Neyman & Scott 1952; McClelland & Silk 1977; Peebles 1980; Scherrer & Bertschinger 1991; Sheth & Saslaw 1994; Sheth 1996b). Recently, with the new ingredient of a universal halo profile found in numerical simulations (Navarro, Frenk & White 1997; Moore et al. 1999; Navarro et al. 2004), interest in the model has been rekindled (Seljak 2000; Ma & Fry 2000b; Peacock & Smith 2000; Scoccimarro et al. 2001). This model is not seen as literally true, but its construc-

tions give plausible estimates for correlation functions because at a given scale, density-weighted statistics are dominated by the highest density systems, the collapsed haloes. The model has been shown to reproduce two- and three-point density correlation functions in simulations, and, with a carefully chosen halo mass function and 'concentration parameter', can be consistent with self-similar stable clustering (Ma & Fry 2000a; Smith et al. 2003). Among its many other applications to weak gravitational lensing, pair velocities, the Lyα forest and CMB foregrounds, we find that the halo model also allows us to address the different behaviours of the continuous mass density and of discrete objects such as galaxies.

The halo model also provides expressions for higher order correlations that modify and extend the programme of higher order perturbation theory, which has successfully predicted skewness and higher order amplitudes on large scales (Fry 1984; Bernardeau 1992; Juszkiewicz, Bouchet & Colombi 1993; Bernardeau et al. 2002). In this paper we re-examine the statistical behaviour of

★E-mail: fry@phys.ufl.edu (JNF); colombi@iap.fr (SC); fosalba@ieec.uab.es (PF); abalaraman@georgiasouthern.edu (AB); szapudi@ifa.hawaii.edu (IS); romain.teyssier@cea.fr (RT)

integral moments of total mass or number counts in the context of the halo model. Our results, formulated directly in position space, complement and extend those of Scoccimarro et al. (2001) in the Fourier domain. In Section 2, we present definitions of the various statistics we need and introduce generating function tools that will be applied in later sections. In Section 3, we apply the probability generating function machinery for a system of identical clusters in the point cluster limit, a model we call the 'naive halo model', to express the statistics of counts in cells in terms of properties of the halo number and halo occupancy distributions. In Section 4, we compare the model to results obtained from numerical simulations. We find that the naive point cluster model describes the qualitative behaviour but fails in quantitative detail, but insight gathered from the model in the generating function formalism is easily applied in the full halo model. This leads us in Section 5 to consider the halo model in its full detail, summing over haloes of different mass, with both halo occupations and halo correlations functions of halo mass. Properly interpreted, the naive point cluster results obtained using the generating function continue to apply when averaged over halo masses and over galaxy positions within a halo. This allows us to extend to small scales, where haloes are resolved, introducing geometric form factors for haloes that can no longer be considered as points. Working directly in space instead of in the Fourier transform domain allows us to exhibit manifestly symmetries under particle exchange at all orders; avoids the necessity to introduce an approximate factoring of window function products $W_1 W_2 W_{12} \approx W_1^2 W_2^2$, etc. and avoids the necessity to make any assumptions or approximations about configuration dependence. Known forms of the halo mass function, bias and occupation number allow us to compute from first principles results in scale-free and specific cosmological models. Section 6 contains a final discussion, and some technical results are included in Appendices.

2 STATISTICAL DEFINITIONS

We study statistics of the continuous mass density and of discrete objects that for convenience we denote as 'galaxies'. For a galaxy number distribution that is a random sampling of a process with a smooth underlying number density field $n(\mathbf{r})$, factorial moments of the number of galaxies in a randomly placed volume directly reflect moments of the underlying continuous density field (Szapudi & Szalay 1993),

$$\langle N^{[k]} \rangle = \bar{N}^k \bar{\mu}_k, \tag{1}$$

where $N^{[k]} = N!/(N-k)! = N(N-1)\ldots(N-k+1)$, and the moments $\bar{\mu}_k$ are volume averages of corresponding moments of the underlying density field,

$$\bar{\mu}_k = \frac{1}{V^k} \int_V d^3 r_1 \cdots d^3 r_k \, \mu_k(\mathbf{r}_1, \ldots, \mathbf{r}_k), \tag{2}$$

$$\langle n(\mathbf{r}_1) \cdots n(\mathbf{r}_k) \rangle = \bar{n}^k \, \mu_k(\mathbf{r}_1, \ldots, \mathbf{r}_k), \tag{3}$$

typically integrated over a spherical volume of radius R. Moments of powers $\langle N^k \rangle$ then contain contributions arising from discreteness; for $k = 2$ through 5 these are

$$\langle N^2 \rangle = \bar{N} + \bar{N}^2 \bar{\mu}_2, \tag{4}$$

$$\langle N^3 \rangle = \bar{N} + 3\bar{N}^2 \bar{\mu}_2 + \bar{N}^3 \bar{\mu}_3, \tag{5}$$

$$\langle N^4 \rangle = \bar{N} + 7\bar{N}^2 \bar{\mu}_2 + 6\bar{N}^3 \bar{\mu}_3 + \bar{N}^4 \bar{\mu}_4, \tag{6}$$

$$\langle N^5 \rangle = \bar{N} + 15\bar{N}^2 \bar{\mu}_2 + 25\bar{N}^3 \bar{\mu}_3 + 10\bar{N}^4 \bar{\mu}_4 + \bar{N}^5 \bar{\mu}_5. \tag{7}$$

In the limit $\bar{N} = \langle N \rangle \gg 1$ the highest power of $\bar{N}$ dominates and $\langle N^k \rangle = \bar{N}^k \bar{\mu}_k$, as for a continuous density; the factorial moment, in removing the lower order or discreteness terms, leaves a discreteness-corrected moment that reflects only spatial clustering. The moments $\bar{\mu}_k$ can be additionally separated into irreducible contributions $\bar{\xi}_k$, as

$$\bar{\mu}_2 = 1 + \bar{\xi}_2, \tag{8}$$

$$\bar{\mu}_3 = 1 + 3\bar{\xi}_2 + \bar{\xi}_3, \tag{9}$$

$$\bar{\mu}_4 = 1 + 6\bar{\xi}_2 + 3\bar{\xi}_2^2 + 4\bar{\xi}_3 + \bar{\xi}_4, \tag{10}$$

$$\bar{\mu}_5 = 1 + 10\bar{\xi}_2 + 10\bar{\xi}_3 + 15\bar{\xi}_2^2 + 10\bar{\xi}_2\bar{\xi}_3 + 5\bar{\xi}_4 + \bar{\xi}_5, \tag{11}$$

also written as 'connected' moments,

$$\langle N^{[k]} \rangle_c = \bar{N}^k \, \bar{\xi}_k. \tag{12}$$

The relations between the $\bar{\mu}_k$ and the $\bar{\xi}_k$ can be summarized in the generating functions $M(t)$ and $K(t) = \log M(t)$ (Fry 1985),

$$M(t) = \sum_{k=0}^{\infty} \frac{1}{k!} \bar{N}^k \bar{\mu}_k t^k, \qquad K(t) = \sum_{k=1}^{\infty} \frac{1}{k!} \bar{N}^k \bar{\xi}_k t^k. \tag{13}$$

With the factors $1/k!$, M and K are sometimes called exponential generating functions of the moments $\bar{\mu}_k, \bar{\xi}_k$. It is often found that the correlations vary with scale roughly as $\bar{\xi}_k \propto \bar{\xi}^{k-1}$. The hierarchical amplitudes S_k are defined by

$$\bar{\xi}_k = S_k \, \bar{\xi}^{k-1}. \tag{14}$$

The normalization of $\bar{\xi}_k$ to S_k then removes much of the dependence of $\bar{\xi}_k$ on scale.

Generating functions provide an interesting connection between discrete and continuous processes. For a continuous variate x with moment generating function $M_c(t) = \langle e^{tx} \rangle$, the generator of a distribution of discrete counts N for which x is the local density is $M_d(t) = M_c(e^t - 1)$ (Fry 1985). This relation of generating functions provides directly the discreteness terms in equations (4)–(7). For discrete counts with probabilities P_N, also useful is the probability generating function

$$G(z) = \sum_{N=0}^{\infty} P_N z^N. \tag{15}$$

For a discrete realization of an underlying continuous number density, $G(z)$ is related to the exponential generating function of factorial moments by $M(t) = G(t+1)$ (Fry 1985; Szapudi & Szalay 1993).

3 CELL COUNTS ON LARGE SCALES: THE POINT CLUSTER MODEL

Using the tools introduced in the previous section we can now construct the generating function of total number count in the point cluster limit. On large scales, we expect that we can consider relatively compact clusters in their entirety to be either inside or outside of V. The total number of galaxies in a volume is then the sum over all the clusters in the volume,

$$N = \sum_{i=1}^{N_h} N_i, \tag{16}$$

where the number of clusters N_h and the number of galaxies N_i in each cluster are chosen randomly and at first we take the cluster occupation numbers N_i to be independent and identically distributed. A similar sum over clusters arises in situations ranging from the

distribution of particle multiplicities in hadron collisions at high-energy accelerators (Finkelstein 1988; Hegyi 1994; Tchikilev 1999) to the distribution of rainfall totals (Rodriguez-Iturbe, Cox & Isham 1987; Cowpertwait 1994; Evin & Favre 2008).

We can characterize the net count distribution directly for small counts and in general using the generating function $G(z)$. Let p_n be the probability of V containing n clusters, and let q_n be the probability that a cluster has n members. Because a cluster with no members is uninteresting, for simplicity we take $q_0 = 0$ here; for the case $q_0 \neq 0$, see Appendix A. Then, to have no count, we must have no clusters; to have total count one, we must have one cluster with one member; to have total count two we can have one cluster with two members or two clusters with one member and so on. The first several probabilities P_N that V contains N total galaxies are then

$$P_0 = p_0 \tag{17}$$

$$P_1 = p_1 q_1 \tag{18}$$

$$P_2 = p_1 q_2 + p_2 q_1^2 \tag{19}$$

$$P_3 = p_1 q_3 + 2 p_2 q_1 q_2 + p_3 q_1^3 \tag{20}$$

$$P_4 = p_1 q_4 + p_2 \left(2 q_1 q_3 + q_2^2\right) + 3 p_3 q_1^2 q_2 + p_4 q_1^4 \tag{21}$$

$$
\begin{aligned}
P_5 &= p_1 q_5 + p_2 \left(2 q_1 q_4 + 2 q_2 q_3\right) \\
&\quad + p_3 \left(3 q_1^2 q_3 + 3 q_1 q_2^2\right) + 4 p_4 q_1^3 q_2 + p_5 q_1^5.
\end{aligned}
\tag{22}
$$

For these first few low-order terms, P_N is the coefficient of z^N in the composition of generating functions $g_h[g_i(z)]$. This is the general result, as can be seen easily from the generating function for the total count probabilities P_N,

$$
\begin{aligned}
G(z) &= \left\langle\!\left\langle z^{N_1 + N_2 + \cdots + N_{N_h}} \right\rangle\!\right\rangle = \left\langle \langle z^{N_i} \rangle^{N_h} \right\rangle \\
&= \left\langle [g_i(z)]^{N_h} \right\rangle = g_h[g_i(z)],
\end{aligned}
\tag{23}
$$

where the double angle brackets indicate an average over both the distributions of cluster occupancy and cluster number (see Szapudi & Szalay 1993).

We can also compute moments directly and using generating functions. The mean of $N = \sum N_i$ is the number of haloes times the average occupation per halo,

$$\langle N \rangle = \langle N_h N_i \rangle = \bar{N}_h \bar{N}_i. \tag{24}$$

The square $N^2 = \sum N_i \sum N_j$ contains N_h terms with $i = j$ and $N_h(N_j - 1)$ terms with $i \neq j$,

$$
\begin{aligned}
\langle N^2 \rangle &= \left\langle N_h N_i^2 + N_h (N_h - 1) N_i N_j \right\rangle \\
&= \bar{N}_h \left(\bar{N}_i + \bar{N}_i^2 \bar{\mu}_{2,i} \right) + \bar{N}_h^2 (1 + \bar{\xi}_{2,h}) \bar{N}_i^2.
\end{aligned}
\tag{25}
$$

Similar direct calculations give

$$
\begin{aligned}
\langle N^3 \rangle &= \Big\langle N_h N_i^3 + N_h (N_h - 1) 3 N_i^2 N_j \\
&\quad + N_h (N_h - 1)(N_h - 2) N_i N_j N_k \Big\rangle
\end{aligned}
\tag{26}
$$

$$
\begin{aligned}
\langle N^4 \rangle &= \Big\langle N_h N_i^4 + N_h (N_h - 1) \left(4 N_i^3 N_j + 3 N_i^2 N_j^2\right) \\
&\quad + N_h (N_h - 1)(N_h - 2)\, 6 N_i^2 N_j N_k \\
&\quad + N_h (N_h - 1)(N_h - 2)(N_h - 3)\, N_i N_j N_k N_l \Big\rangle
\end{aligned}
\tag{27}
$$

$$
\begin{aligned}
\langle N^5 \rangle &= \Big\langle N_h N_i^5 + N_h (N_h - 1) \left(5 N_i^4 N_j + 10 N_i^3 N_j^2\right) \\
&\quad + N_h^{[3]} \left(10 N_i^3 N_j N_k + 15 N_i^2 N_j^2 N_k\right) \\
&\quad + N_h^{[4]}\, 10 N_i^2 N_j N_k N_l + N_h^{[5]}\, N_i N_j N_k N_l N_m \Big\rangle,
\end{aligned}
\tag{28}
$$

and from these, the discreteness corrected, connected moments of total count are

$$\bar{\xi}_2 = \bar{\xi}_{2,h} + \frac{\bar{\mu}_{2,i}}{\bar{N}_h} \tag{29}$$

$$\bar{\xi}_3 = \bar{\xi}_{3,h} + \frac{3 \bar{\mu}_{2,i} \bar{\xi}_{2,h}}{\bar{N}_h} + \frac{\bar{\mu}_{3,i}}{\bar{N}_h^2} \tag{30}$$

$$\bar{\xi}_4 = \bar{\xi}_{4,h} + \frac{6 \bar{\mu}_{2,i} \bar{\xi}_{3,h}}{\bar{N}_h} + \frac{\left(4 \bar{\mu}_{3,i} + 3 \bar{\mu}_{2,i}^2\right) \bar{\xi}_{2,h}}{\bar{N}_h^2} + \frac{\bar{\mu}_{4,i}}{\bar{N}_h^3} \tag{31}$$

$$
\begin{aligned}
\bar{\xi}_5 &= \bar{\xi}_{5,h} + \frac{10 \bar{\mu}_{2,i} \bar{\xi}_{4,h}}{\bar{N}_h} + \frac{\left(10 \bar{\mu}_{3,i} + 15 \bar{\mu}_{2,i}^2\right) \bar{\xi}_{3,h}}{\bar{N}_h^2} \\
&\quad + \frac{\left(10 \bar{\mu}_{2,i} \bar{\mu}_{3,i} + 5 \bar{\mu}_{4,i}\right) \bar{\xi}_{2,h}}{\bar{N}_h^3} + \frac{\bar{\mu}_{5,i}}{\bar{N}_h^4},
\end{aligned}
\tag{32}
$$

etc. Clearly, the effort and complexity increase at each order. Identical results are obtained by the composition of generating functions in equation (23). The general term can be obtained from the generating function $K(t)$ for moments of total counts. Using the relation $M(t) = G(t + 1)$, the composition of probability generating functions in equation (23) is also a composition of moment generating functions,

$$
\begin{aligned}
K(t) &= \log[M(t)] = \log[G(t + 1)] \\
&= \log\{g_h[g_i(t + 1)]\} = \log\{g_h[M_i(t)]\} \\
&= \log\{M_h[M_i(t) - 1]\} = K_h[M_i(t) - 1],
\end{aligned}
\tag{33}
$$

from which it is clear that $\bar{\xi}_k$ continues to depend to all orders on the connected moments $\bar{\xi}_{k,h}$ of halo number as the coefficients in K_h and the raw moments $\bar{\mu}_{k,i}$ of the halo occupation distribution as the coefficients in M_i. The generating function in equation (33) and the expressions for moments of counts in equations (29)–(32) plus extension to higher orders constitute the main result of the point cluster model. The point cluster results are independent of the internal details of halo profiles or concentrations. The general expression for $\bar{\xi}_k$ contains contributions from occupation number moments of order 1 through k and halo correlations of order 1 through k; in $\bar{\xi}_5$, the first term arises from five objects in five separate haloes, the last from occupancy five in a single halo, while other terms represent four haloes with occupancies (2, 1, 1, 1); three haloes with occupancies (3, 1, 1) and (2, 2, 1); and two haloes with occupancies (3, 2) and (4, 1). The numerical factors represent the number of equivalent halo assignments. The sum of the combinatoric factors of a given $\bar{\xi}_{n,h}$ in the expression for $\bar{\xi}_k$ is known as Stirling numbers of the second kind, $S(n, k)$, the number of ways of putting n distinguishable objects into k cells with no cells empty (Scherrer & Bertschinger 1991). Here, they are produced from a generating function in a manner such that any term desired can be easily produced by an algebraic manipulator.

Some special cases are useful to consider. For single-element clusters, $N_i = 1$ with probability 1, the occupation moments are $\bar{\mu}_1 = 1$ and $\bar{\mu}_k = 0$ for $k \geq 2$, galaxies are haloes and galaxy correlations are halo correlations, $\bar{\xi}_k = \bar{\xi}_{k,h}$. For Poisson occupation number, the occupation moments are all $\bar{\mu}_{k,i} = 1$, and the halo model expressions reproduce the discreteness terms of equations (4)–(7). This is the locally Poisson realization of a distribution with spatially varying $n(\mathbf{r})$. For uncorrelated cluster positions, irreducible moments arise only from objects in the same halo; in this case the halo number N_h has a Poisson distribution, and the

single-halo contribution to the count moment,

$$\bar{\xi}_k^{1h} = \frac{\bar{\mu}_{k,i}}{\bar{N}_h^{k-1}}, \tag{34}$$

is often called the Poisson term. The composition of generating functions for a Poisson halo distribution was studied by Sheth (1995a,b). The point cluster model varies from the halo clustering limit to the Poisson limit as a function of scale. Typically, the two-point function behaves as $\bar{\xi}(r) \sim r^{-\gamma}$ with $\gamma \approx 2$, and higher order correlations scale hierarchically, as $\bar{\xi}_k = S_k \bar{\xi}^{k-1}$, with nearly constant S_k. Since $\bar{N}$ grows as R^3, the dominant contribution to $\bar{\xi}_k$ on large scales then comes from the halo correlation, $\bar{\xi}_k \approx \bar{\xi}_{k,h}$, but on scales where $\bar{N}\bar{\xi} \lesssim 1$, the point cluster model gives the one-halo term in equation (34). In this regime total number count moments have hierarchical correlations, with $S_k = \bar{\mu}_{k,i}/\bar{\mu}_2^{k-1}$.

Many common statistical models are constructed starting with a Poisson halo number distribution, so that $\bar{\xi}_{k,h} = 0$ for $k \geq 2$, and equation (34) holds exactly. If the occupancy distribution is also Poisson, $\bar{\mu}_{k,i} = 1$, then $S_k = 1$ for all k ($S_1 = S_2 = 1$ always), saturating constraints $S_{2m}S_{2n} \geq S_{m+n}^2$ arising from the Schwarz inequality; this is a realization of the minimal hierarchical model of Fry (1985). Other examples of compound Poisson distributions include the negative binomial distribution, which is the composition of a Poisson cluster distribution with a logarithmic occupation distribution (Sheth 1995b), and the thermodynamic or quasi-equilibrium distribution of Saslaw & Hamilton (1984), which is the composition of a Poisson cluster distribution with a Borel occupation distribution (Saslaw 1989; Sheth & Saslaw 1994; Sheth 1995a).

There is one generalization that is also useful, where the total number of objects is the sum of contributions from two independent populations, $N = N_c + N_b$ such as the sum of a strongly clustered population plus a weakly clustered 'background' (cf. Soneira & Peebles 1977). In this case the cumulant moments $\bar{\xi}_k$ are simply additive,

$$\bar{N}^k \bar{\xi}_k \to \bar{N}_c^k \bar{\xi}_{c,k} + \bar{N}_b^k \bar{\xi}_{b,k}. \tag{35}$$

If the background contributes to the total count, $\bar{N} = \bar{N}_c + \bar{N}_b$, but not to higher order moments, we have

$$\bar{\xi}_k = \frac{\bar{N}_c^k}{(\bar{N}_b + \bar{N}_c)^k} \bar{\xi}_{c,k} = f_c^k \bar{\xi}_{c,k}, \tag{36}$$

where f_c is the fraction of clustered objects. Although the correlations are diluted, this says that the amplitudes for $k \geq 3$ are amplified, $S_k = S_{c,k}/f_c^{k-2}$.

4 NUMERICAL RESULTS

In this section we compare the model to statistics of galaxies and haloes identified within the setting of a single numerical simulation. The sample we use is the same one analysed in Colombi, Chodorowski & Teyssier (2007, hereafter CCT), where many more details can be found. The simulation is performed with the adaptive mesh refinement (AMR) code RAMSES (Teyssier 2002), assuming a standard Λ cold dark matter cosmology with $\Omega_m = 0.3$, $\Omega_\Lambda = 0.7$, $H_0 = 100\,h\,\mathrm{km\,s^{-1}\,Mpc^{-1}}$ with $h = 0.7$, and a normalization $\sigma_8 = 0.93$, where σ_8 is the root mean square initial density fluctuations in a sphere of radius $8\,h^{-1}$ Mpc extrapolated linearly to the present time. The simulation contains 512^3 dark matter particles on the AMR grid, initially regular of size 512^3, in a periodic cube of size $L_{box} = 200\,h^{-1}$ Mpc; the mass of a single particle is then 7.09×10^9 M$_\odot$. Additional refinement is allowed during runtime: cells containing more than $N_{AMR} = 40$ particles are divided using

the standard AMR technique with a maximum of seven levels of refinement.

A halo catalogue, E_h, and a 'galaxy' (subhalo) catalogue, E_h, are extracted from the final state of the simulation using the publically available software ADAPTAHOP (Auber, Pichon & Colombi 2004); details of the procedure can again be found in CCT. We use the number of dark matter substructures in each halo detected by ADAPTAHOP as a proxy for the galaxy distribution. A halo can contain one or more galaxies: a single component halo hosts one galaxy (or is its own substructure), and an N-component halo hosts N galaxies. The substructure distribution differs somewhat from that of galaxies (see the discussions in CCT and Weinberg et al. 2008), but it provides a discrete number count distribution that is useful to test how the behaviour of the discrete halo model differs from that of the continuous mass distribution.

Fig. 1 shows the distributions of halo mass $f(m)$ and of occupation number P_N for the full halo catalogue. The range of masses covers almost four decades; the largest halo contains 53 substructures. Moments of these distributions give the occupation moments $\bar{\mu}_k$ that appear in equations (29)–(32) and the point halo hierarchical amplitudes $S_k = \bar{\mu}_k/\bar{\mu}_2^{k-1}$. For comparison, smooth lines in the figure show the Press–Schechter (solid line) and Sheth–Tormen (dotted line) mass functions, plotted for $\delta_c = 1.50$. The Press–Schechter and Sheth–Tormen mass distributions provide a good representation of the mass function for $M \geq 10^{12}$ M$_\odot$, rising with mass a little more weakly than $1/M$ towards small masses and with an exponential cut-off at large mass. The number distribution behaves as a power law, $P_N \sim 1/N^p$, with p in the range 2.0–2.4. The subclump finder ADAPTAHOP identifies haloes as connected regions with density contrast larger than $\delta > 80$ employing a standard SPH softening of the particle distribution with $N_{SPH} = 64$ neighbours (see e.g. Monaghan 1992). This, along with the mass resolution of the structures resolved by RAMSES, controlled by the value of N_{AMR}, leads to the rather soft small-M cut-off on the halo mass function in Fig. 1 and also the low value of δ_c.

The full samples E_h and E_g contain 50 234 haloes and 64 316 'galaxies', respectively. Most haloes have a single component; the average number of substructures per halo is $\bar{N}_i = 1.28$. From these two parent catalogues, we apply various mass thresholdings to extract subsamples from E_h and E_g that we denote as $E_h(M_{min}, M_{max})$
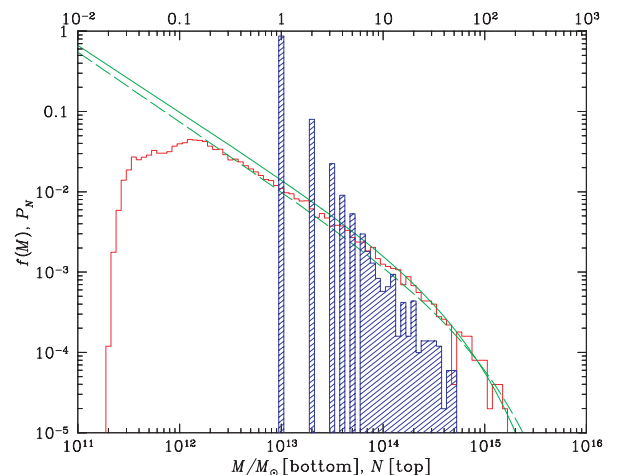

Figure 1. Distribution of halo masses $f(M)$ (histogram; bottom scale) as a function of M and substructure occupation number probability P_N (shaded histogram; top scale) as a function of N. The solid and dashed curves show the Press–Schechter and Sheth–Tormen mass functions.

Table 1. Details of the catalogues extracted from RAMSES. The two first columns give the halo mass range, $M_{min} < M_h < M_{max}$ (in units of $M_\odot$); the third and fourth columns give the number of objects in the halo and substructure catalogues; and the fifth and sixth columns give the average number of substructures and dark matter particles per halo.

M_{min}	M_{max}	N_{haloes}	N_{subs}	$\bar{N}_i^{subs}$	$\bar{N}_i^{dm}$
0	∞	50 234	64 316	1.28	967
0	10^{14}	49 740	59 203	1.19	636
5×10^{11}	∞	43 482	57 564	1.32	1109
5×10^{11}	10^{14}	42 988	52 451	1.22	727
4×10^{12}	∞	11 934	24 918	2.09	3441
4×10^{12}	10^{14}	11 440	19 805	1.73	2108
10^{14}	∞	494	5113	10.35	34 315

where M_{min} and M_{max}, given in solar masses, correspond to minimum and maximum mass thresholds of the host haloes, respectively. We use these subcatalogues to test the variation of halo clustering with mass. The different realizations break down as follows.

(i) The full sample separated into 'light' and 'massive' halo subsamples, $E_h(0, \infty) \equiv E_h \equiv E_h(0, 10^{14}) + E_h(10^{14}, \infty)$, and the substructure counterparts.

(ii) A catalogue of haloes with masses larger than 5×10^{11} $M_\odot$, which avoids the strongest rolloff at small mass, separated likewise into two subsamples, $E_h(5 \times 10^{11}, \infty) \equiv E_h(5 \times 10^{11}, 10^{14}) + E_h(10^{14}, \infty)$, and the substructure counterparts.

(iii) A catalogue of haloes with masses larger than 4×10^{12} $M_\odot$, which avoids essentially all of the rolloff at small mass, separated likewise into two subsamples, $E_h(4 \times 10^{12}, \infty) \equiv E_h(4 \times 10^{12}, 10^{14}) + E_h(10^{14}, \infty)$, and the substructure counterparts.

Table 1 summarizes subcatalogue information.

From the distribution of mass and the catalogue of haloes and subhaloes in the simulation we compute correlation statistics $\bar{\xi}_k$ for $k = 2$–5. Fig. 2 shows the variance, or volume-averaged two-point correlation function $\bar{\xi}_2$, evaluated for spherical volumes of radius R
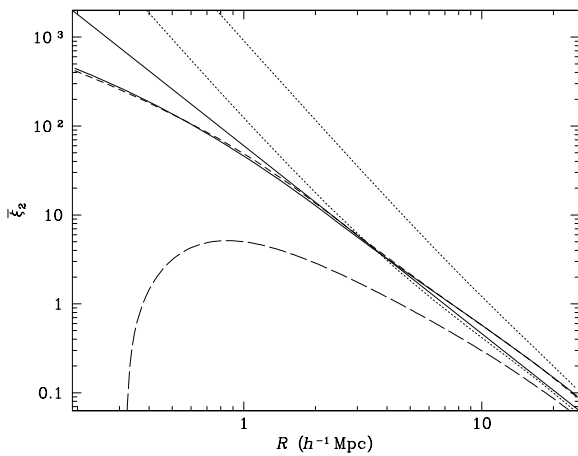
Figure 2. Variance $\bar{\xi}_2(R)$ for mass (solid line) and for halo number (long-dashed line) measured for spheres of radius R in numerical simulations compared with the halo model. Dotted lines show the point cluster model of equation (29); the upper line shows only the contribution of particles in haloes, while the lower dotted line includes particles not in haloes as an unclustered background. The short-dashed line includes a bias $b = 1.25$ between mass and haloes on large scales and the effects of resolved haloes on small scales.
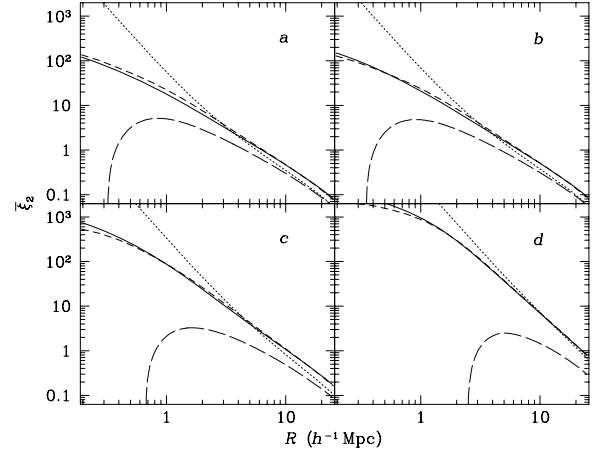
Figure 3. Cell count variance $\bar{\xi}_2(R)$ in spheres of radius R obtained from numerical simulations compared with the halo model. Solid lines show $\bar{\xi}_2$ measured for galaxies (substructures) and long-dashed lines show $\bar{\xi}_{2,h}$ measured for haloes identified in the simulations for the four subcatalogues. Results for all haloes are presented in panel (*a*), $M > 5 \times 10^{11}$ in panel (*b*), 4×10^{12} in panel (*c*) and 10^{14} $M_\odot$ in panel (*d*). The dotted lines show the point cluster model of equation (29), and the short-dashed lines include bias and resolved haloes.

as a function of R, for dark matter, or mass (solid line), and for haloes (long-dashed line). Dotted lines show the predictions of the point cluster model: the upper line for only the mass in haloes, and the lower line including mass not contained in haloes as an unclustered background, as in equation (36), with $f_c = \sum M_h/M_{tot} = 0.36$. Finally, the short-dashed line includes two additional aspects from the full halo model, a modest relative bias factor $b = 1.22$ between mass and haloes on large scales, and the effects of resolved haloes, detailed in Section 5.

Panels in Fig. 3 show the second moment evaluated for substructure 'galaxies' $\bar{\xi}_{2,g}$ (solid lines) and for haloes, $\bar{\xi}_{2,h}$ (long-dashed lines) for the four inclusive catalogues: haloes of all masses, with $M > 5 \times 10^{11}$ $M_\odot$, with $M > 4 \times 10^{12}$ $M_\odot$ and with $M > 10^{14}$ $M_\odot$, as identified in the caption. Dotted curves show the predictions of the simple point cluster model. Although it has shortcomings in detail, on scales of a few Mpc the point cluster model with no adjustments reproduces the trends with scale and from catalogue to catalogue to within a factor of 2 or so over four decades of correlation strength. Dashed curves show a quantitative improvement with a very modest adjustment of parameters, relative bias factors of 1.2 or 1.3 and occupation moments adjusted by a factor of 2, as given in the middle columns in Table 2. For radius smaller than $1\,h^{-1}$Mpc finite halo size starts to become important. The mass threshold $M > 5 \times 10^{11}$ $M_\odot$ removes only haloes containing a single substructure (the smallest halo containing two substructures has a mass 8×10^{11} $M_\odot$), and so affects only the mean $\bar{N} = \langle N \rangle$ but none of the higher factorial moments $\langle N^{[k]} \rangle$, just as for an unclustered background population as in equation (36). Thus, in the regime where the normalized moment is large, $\bar{\xi}_k \gg 1$, it is simply rescaled, $\bar{\xi}_k'/\bar{\xi}_k = (\bar{N}/\bar{N}')^k$. This is apparent for the data plotted in Fig. 2, where for the smallest cells $\bar{\xi}_2$ for the $E_g(5 \times 10^{11})$ subsample is larger than that for the full E_g sample by a factor of 1.249, very close to the number ratio $(64\,316/57\,564)^2 = 1.246$. The next mass threshold, $M > 4 \times 10^{12}$ $M_\odot$, removes doubly and also triply occupied haloes (the smallest halo containing three substructures has a mass 1.8×10^{12} $M_\odot$), and so this threshold changes the shape of $\bar{\xi}_2$ and $\bar{\xi}_3$.

Table 2. Correlation parameters for 'galaxies' and mass. The first five columns show values in the simple point cluster model, in which all haloes are identical, using the simulation halo distributions p_N and $f(M)$; the next five columns show fit values (f); and the last five columns show values computed in the detailed halo model (m).

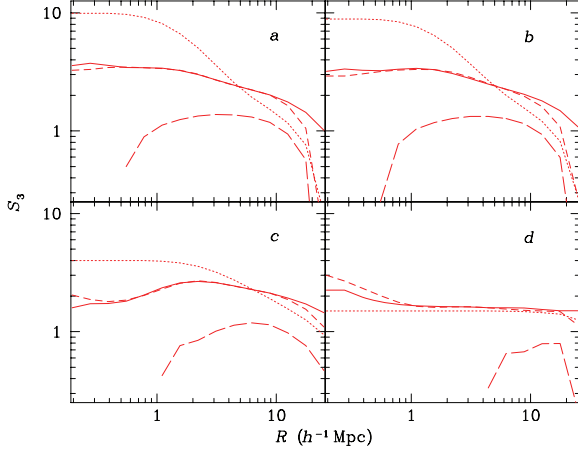| Sample	b/b_h	$\bar{\mu}_2$	S_3	S_4	S_5	b/b_h^f	$\bar{\mu}_2^f$	S_3^f	S_4^f	S_5^f	b/b_h^m	$\bar{\mu}_2^m$	S_3^m	S_4^m	S_5^m
Dark matter (mass)	1	4.00	7.18	93.0	1460	1.25	1.96	7.2	93	1460	1.71	34.3	6.8	101	2450
All haloes	1	1.35	9.92	168	3360	1.22	0.60	3.4	26	330	1.39	10.6	7.15	115	2980
$m > 5 \times 10^{11}\,M_\odot$	1	1.46	8.88	134	2410	1.23	0.70	3.4	25	300	1.37	6.95	5.24	59.5	1050
$m > 4 \times 10^{12}\,M_\odot$	1	2.10	4.00	26.8	212	1.34	1.27	2.3	10	68	1.30	3.03	3.27	22.4	239
$m > 1 \times 10^{14}\,M_\odot$	1	1.50	1.50	2.93	6.59	1.36	1.09	1.7	4.0	13	1.12	1.54	1.41	3.01	9.30

Figure 4. Hierarchical amplitudes $S_3(R)$ from numerical simulations for substructure 'galaxy' catalogues (solid lines) and for the corresponding haloes (long-dashed lines) The dotted lines show the naive point cluster model, and the short-dashed lines include bias and resolved haloes. Panels show the four different subcatalogues, as in Fig. 3.

Figure 5. Hierarchical amplitudes $S_k(R)$ for mass density from numerical simulations for $k = 3$, 4 and 5 (bottom to top). Solid lines show S_k measured for mass and long-dashed lines show S_k for haloes. Dotted lines show the naive point cluster model expressions in equations (30)–(32) and same results but adjusted for a weakly clustered background (not contained in haloes). The short-dashed lines also include a bias factor on large scales and the effects of resolved haloes on small scales, as detailed in Section 5.

Panels in Fig. 4 show the hierarchical amplitude S_3 for the four subhalo catalogues (solid lines), and for the corresponding halo catalogues (long-dashed lines). Finite volume limitations are apparent at large scales, and the $E_h(10^{14})$ sample is not large enough for a reliable third moment on almost any scale. Dotted lines show the naive point cluster model. Again, the first mass cut $M > 5 \times 10^{11}\,M_\odot$ removes only haloes containing a single substructure from the full catalogue, changing only the mean count; and on the smallest scales the expected scaling $S_3'/S_3 = \bar{N}'/\bar{N} = 57\,563/64\,316 = 0.895$ is again satisfied.

Fig. 5 shows the amplitudes S_3, S_4 and S_5 for dark matter (solid lines) and for haloes (long-dashed lines). Fig. 6 shows the S_k for substructures (solid lines) and for haloes (long-dashed lines), for the entire E_h halo sample. The naive point cluster model agrees with the simulations qualitatively but not quantitatively. One possible explanation is that halo occupation is correlated with environment, and a modest adjustment of the point cluster parameters gives a good fit. Table 2 shows the naive point cluster model result using occupation probabilities p_N and the halo mass function $n(M)$ from the simulations, and also the result of adjusting fit parameters. In the point cluster model, the parameters are factorial moments $\bar{\mu}_k = \langle N^{[k]} \rangle / \bar{N}^k$ for galaxies and $\bar{\mu}_k = \langle M^k \rangle / \bar{M}^k$ for mass, computed for the haloes identified in the simulation. The quantity identified as 'b' is the large-scale relative bias between galaxies and haloes, $b^2 = \bar{\xi}_{2,g} / \bar{\xi}_{2,h}$.
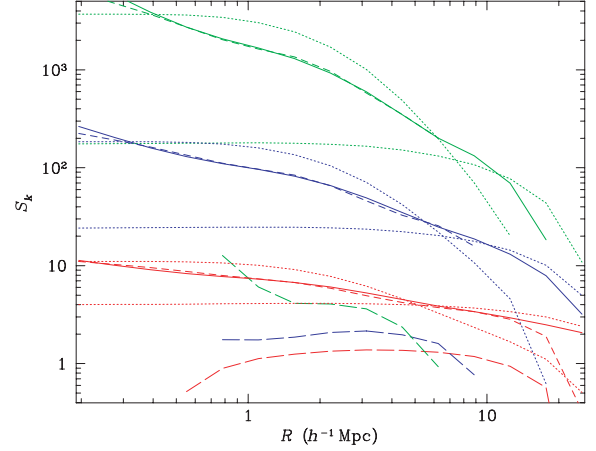
5 THE FULL HALO MODEL

To extend our understanding we turn to the context of the recently developed phenomenological halo model (Seljak 2000; Ma & Fry 2000b; Peacock & Smith 2000; Scoccimarro et al. 2001; Cooray
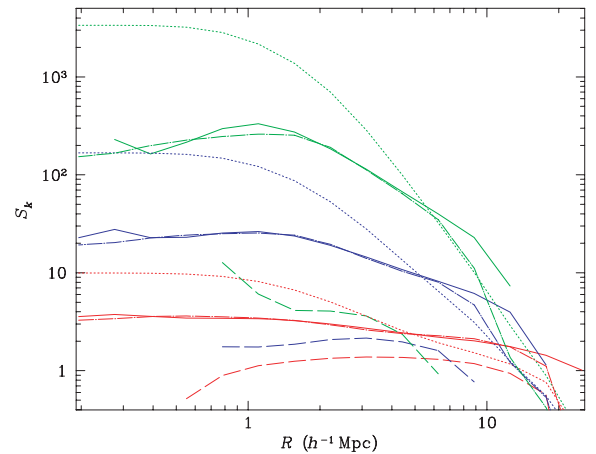

Figure 6. Hierarchical amplitudes $S_k(R)$ for galaxy number count measured in from numerical simulations for $k = 3$, 4 and 5 (bottom to top). Solid lines show galaxy (substructure) S_k, and long-dashed lines show halo $S_{k,h}$. Dotted lines show the point cluster model expressions in equations (30)–(32).

& Sheth 2002), in which clustering on small scales is derived from the mass function, profiles and clustering properties of dark matter haloes. Numerical simulations have suggested haloes have a universal density profile (Navarro et al. 1997; Moore et al. 1999; Navarro et al. 2004),

$$\frac{\rho(r)}{\bar{\rho}} = A u \left(\frac{r}{r_s} \right), \tag{37}$$

where the scale r_s and amplitude A are functions of the halo mass. In particular, r_s is related to the virial radius r_{200}, within which the average density is 200 times the mean, by a 'concentration parameter' $c(m)$, $r_s = r_{200}/c$; this then also determines the amplitude A. For a large cluster, say $m = 10^{15}$ M$_\odot$, the virial radius is about $3\,h^{-1}$ Mpc; and with $c \approx 6$ the scale radius is $r_s \approx 500\,h^{-1}$ kpc. Thus, at roughly Mpc and smaller scales we begin to resolve clusters, and we expect to have to replace the point cluster model with the full halo model.

The halo mass function is conveniently written as a function of the dimensionless overdensity $\nu = \delta_c/\sigma(m)$, where δ_c is the threshold overdensity that leads to a collapsed halo, often $\delta_c = 1.68$, and $\sigma^2(R)$ is the mean square mass fluctuation within a sphere of radius R evaluated for the linearly evolved input power spectrum. Specifically,

$$\sigma^2(m) = \int \frac{\mathrm{d}^3 k}{(2\pi)^3} \, P(k) \, W^2(kR), \tag{38}$$

where $W(x) = 3(\sin x - x \cos x)/x^3$ is the Fourier window corresponding to a real-space top-hat window function, and $m = 4\pi\bar{\rho}R^3/3$. In terms of ν, the density of haloes of mass M is then written as

$$\frac{\mathrm{d}n}{\mathrm{d}m} = \frac{\mathrm{d}(\ln \nu)}{\mathrm{d}(\ln m)} \frac{\bar{\rho}}{m^2} \, \nu f(\nu). \tag{39}$$

The Gaussian distribution function $f(\nu)$ of Press & Schechter (1974, hereafter PS) and the refinement of Sheth & Tormen (1999, hereafter ST) both have

$$\nu f(\nu) = 2A \left[1 + (q\nu^2)^{-p} \right] \left(\frac{q\nu^2}{2\pi} \right)^{1/2} \mathrm{e}^{-q\nu^2/2}. \tag{40}$$

The normalization A is chosen so that $\int \mathrm{d}\nu f(\nu) = 1$ and is independent of q. The Press–Schechter function has $q = 1$, $p = 0$, $A = 1/2$; the Sheth–Tormen form has $q = 0.707$, $p = 0.3$, $A \approx 0.322\,18$.

5.1 One-halo term in the point cluster limit

In the point cluster limit of the full halo model, the sum over haloes in equation (16) and the resulting composition of generating functions in equation (23) remain true, but the calculation now includes an average over the distribution of halo masses as well as over halo occupation and halo count, both of which now differ with halo mass. The resulting order-k connected correlation function is again a sum of contributions from a single halo to k different haloes, just as in equations (29)–(32), with the same coefficients. For the one-halo term of the order-k moment in the full halo model, the average over all haloes includes an average over the halo mass function $\mathrm{d}n/\mathrm{d}m$,

$$\bar{\xi}_k^{1h} = \frac{\langle N_i^{[k]} \rangle}{\langle N_i \rangle^k} \rightarrow \frac{\int \mathrm{d}m \, (\mathrm{d}n/\mathrm{d}m) \, V \, \langle N^{[k]}(m) \rangle}{\left[\int \mathrm{d}m \, (\mathrm{d}n/\mathrm{d}m) \, V \, \langle N(m) \rangle \right]^k}, \tag{41}$$

where $N(m) = N_i(m)$ is the occupancy of a halo of mass m. The factor in brackets in the denominator is

$$\int \mathrm{d}m \, \frac{\mathrm{d}n}{\mathrm{d}m} \, V \, \langle N(m) \rangle = \bar{n}_h V \, \langle N_i \rangle = \bar{N}_h \bar{N}_i = \bar{N}, \tag{42}$$

where $\bar{n}_h$ is the number density of all haloes, $\bar{N}_h = \bar{n}_h V$ is the mean number of haloes in V and $\bar{N}_i$ is the average occupation over haloes of all masses; and the numerator is

$$\int \mathrm{d}m \, \frac{\mathrm{d}n}{\mathrm{d}m} \, V \, \langle N^{[k]}(m) \rangle = \bar{n}_h V \left\langle N_i^{[k]} \right\rangle = \bar{N}_h \bar{N}_i^k \bar{\mu}_{k,i}. \tag{43}$$

The one-halo term of the full halo model thus produces the same result as the previous point cluster result, $\bar{\xi}_k^{1h} = \bar{\mu}_{k,i}/\bar{N}_h^{k-1}$, with occupation moment

$$\bar{\mu}_{k,i} = \frac{\int \mathrm{d}m \, (\mathrm{d}n/\mathrm{d}m) \langle N^{[k]}(m) \rangle \, / \int \mathrm{d}m \, (\mathrm{d}n/\mathrm{d}m)}{\left[\int \mathrm{d}m \, (\mathrm{d}n/\mathrm{d}m) \, \langle N(m) \rangle \, / \int \mathrm{d}m \, (\mathrm{d}n/\mathrm{d}m) \right]^k}. \tag{44}$$

We can compute occupation moments $\bar{\mu}_k$ for mass from first principles by taking number N to be proportional to mass (the number of hydrogen atoms or dark matter particles), $N \propto m$ and $N^{[k]} \propto m^k$ (with no discreteness terms). From (44), these are

$$\bar{\mu}_k = \frac{\left[\int \mathrm{d}m \, (\mathrm{d}n/\mathrm{d}m) \, m^k \right] \left[\int \mathrm{d}m \, (\mathrm{d}n/\mathrm{d}m) \right]^{k-1}}{\left[\int \mathrm{d}m \, (\mathrm{d}n/\mathrm{d}m) \, m \right]^k}, \tag{45}$$

with corresponding hierarchical amplitudes

$$S_k = \frac{\bar{\mu}_k}{\bar{\mu}_2^{k-1}} = \frac{\left[\int \mathrm{d}\nu \, f(\nu) \, m^{k-1} \right] \left[\int \mathrm{d}\nu \, f(\nu) \right]^{k-2}}{\left[\int \mathrm{d}\nu \, f(\nu) \, m \right]^{k-1}} \tag{46}$$

over the range of scales where the one-halo term dominates but haloes are not resolved. In this case, results are determined entirely by the mass function, which in turn is related to the primordial power spectrum. For a power-law power spectrum, with $\nu = (m/m_1)^{(3+n)/6}$, and with the Press–Schechter and Sheth–Tormen forms of the mass functions, the integrals can be done analytically, giving

$$S_k = \frac{I(k) \, [I(1)]^{k-2}}{[I(2)]^{k-1}}, \tag{47}$$

where

$$I(k) = \Gamma \left[\frac{3(k-1)}{3+n} + \frac{1}{2} \right] + 2^{-p} \, \Gamma \left[\frac{3(k-1)}{3+n} + \frac{1}{2} - p \right], \tag{48}$$

independent of q. For a Poisson cluster distribution (on small scales cluster correlations are unimportant) and for the Press–Schechter mass function, this expression was also obtained by Sheth (1996b). For the Press–Schechter mass function, which has $p = 0$, and for spectral index $n = 0$ this gives the particularly simple result $S_k = (2k - 3)!!$. Results for power-law spectra are shown in Fig. 7, together with results from numerical simulations by Colombi, Bouchet & Hernquist (1996) (plotted are the values of S_k measured at $\bar{\xi} = 100$, but values at $\bar{\xi} = 10$ or $\bar{\xi} = 1$ differ by less than the error bars). The Sheth–Tormen mass function appears to agree poorly with the numerical results; this is one instance where the observed behaviour seems to prefer the Press–Schechter form, at least for n not too negative. However, the Sheth–Tormen function is relatively more weighted towards smaller masses, and in numerical simulations there is always a smallest mass that can be considered. Thus, we examine the results of a small mass cut-off in the integral, of 10^{-4} and 10^{-2} in units of the mass m_1 at which $\nu(m_1) = 1$. A 10^{-4} cut-off mass has little effect on PS but is significant for ST, and a 0.01 cut-off has a significant effect on both. In the simulations, the ratio of the particle mass to the non-linear mass is typically in the range 0.001–0.01, and the ST mass function with a moderate low-mass cut-off does agree with the simulations results, at least for $-1 < n < 1$. As n becomes more negative, all the halo model curves rise much more rapidly than the trend seen in the simulation results. This may reflect an increasing difficulty in simulating negative values of n (cf. Jain & Bertschinger 1998).
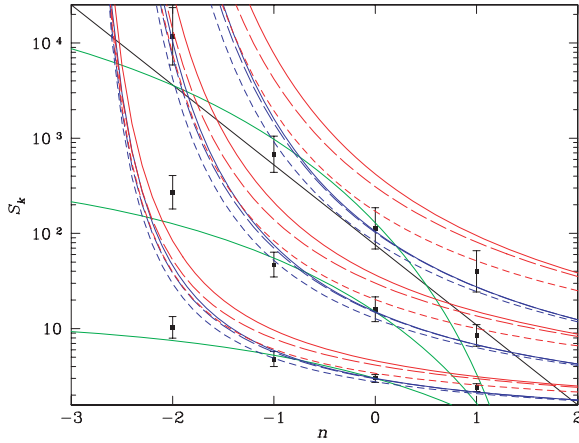
Figure 7. Amplitudes S_k for $k = 3, 4, 5$ (bottom to top) as a function of spectral index n for power-law spectra. For each k there are two sets of curves; the lower set (blue in colour) shows results for the Press–Schechter mass function, and the upper set (red in colour) for Sheth–Tormen, computed from equation (46). Solid lines show S_k integrating over all masses; long-dashed curves have a lower mass cut-off $m > 10^{-4}$; and short-dashed curves have $m > 10^{-2}$, in units of the mass m_1 at which $\nu(m_1) = 1$. The dot–dashed (green) curves show the predictions of hyperextended perturbation theory (Scoccimarro & Frieman 1999). Symbols with error bars show results from numerical simulations (Colombi et al. 1996).

For statistics of galaxy number counts, we must average over moments of halo occupation number,

$$S_k = \frac{\left[\int d\nu \, f(\nu) \langle N^{[k]}(m) \rangle / m \right] \left[\int d\nu \, f(\nu) \, \langle N(m) \rangle / m \right]^{k-2}}{\left[\int d\nu \, f(\nu) \langle N^{[2]}(m) \rangle / m \right]^{k-1}} \quad (49)$$

(the factor $1/m$ remains from the PS or ST halo mass function). In simulations, in general it is found the mean number of galaxies $\langle N(m) \rangle$ grows more slowly than linearly in mass. Models have included a power law, $\langle N(m) \rangle = (m/m_1)^\beta$, with $\beta \lesssim 1$ and perhaps with a minimum mass cut-off m_0; a broken two-power-law model (Berlind & Weinberg 2002) and a similarly behaved but smoothly interpolated function (Berlind et al. 2003). Substructures or sub-halo occupation numbers exhibit a similar behaviour, but perhaps with $\beta \to 1$ at high mass (Kravtsov et al. 2004). Higher order correlations also require higher order moments of the halo occupation distribution, which are typically sub-Poisson at small N, with $\langle N(N-1)(m) \rangle < \langle N(m) \rangle^2$. From semi-analytic galaxy formation considerations, Scoccimarro et al. (2001) extend to higher orders by assuming a binomial distribution, also used by Kravtsov et al. (2004). However, a representation of the galaxy number count distribution as a central galaxy plus a Poisson distribution of satellites (Berlind et al. 2003; Kravtsov et al. 2004; Zheng et al. 2005; Zheng & Weinberg 2007; Zheng, Coil & Zehavi 2007; Zheng et al. 2009) is becoming increasingly popular. In this representation, both central and satellite distributions are characterized entirely by their means $\langle N_c \rangle = \bar{N}_c$ and $\langle N_s \rangle = \bar{N}_s$. Since N_c takes on only the values 0 and 1, so that for any positive power $\langle N_c^p \rangle = \bar{N}_c$, and since for a Poisson satellite distribution $\langle N_s^{[k]} \rangle = \bar{N}_s^k$, the factorial moments of halo occupancy are

$$\langle N^{[k]} \rangle = \bar{N}_s^k + k \, \bar{N}_c \bar{N}_s^{k-1}. \quad (50)$$

The central object can be modelled as a sharp or smoothed step function (Berlind et al. 2003), and Zheng et al. (2005) present expressions for moments with parameters extracted from simulations.

A main import of all models is that moments of occupation number grow more slowly than linearly with mass, a behaviour that we model as the simpler form $N(m) \sim m^\beta$ with $\beta \lesssim 1$. With the Sheth–Tormen mass function and with no small-mass cut-off, S_k for number counts is again a ratio of Γ-functions,

$$S_k = \frac{I_\beta(k) \, [I_\beta(1)]^{k-2}}{[I_\beta(2)]^{k-1}}, \quad (51)$$

where now

$$I_\beta = \Gamma \left[\frac{3\beta(k-1)}{(3+n)} + \frac{1}{2} \right] + 2^{-p} \Gamma \left[\frac{3\beta(k-1)}{(3+n)} + \frac{1}{2} - p \right]. \quad (52)$$

We can use the Poisson model to obtain the occupancy probability distribution averaged over all haloes. For a Poisson distribution with mean $\mu(m)$, the probability p_N for a halo of mass m to contain N galaxies (or N satellite galaxies) is $p_N = \mu^N e^{-\mu}/N!$. Averaged over the power-law portion of the Press–Schechter mass function $dn/dm \sim \nu/m^2$, with the integral cut off by the Poisson exponential $e^{-\mu}$ before the exponential cut-off in the mass function is reached, the probability p_N of N objects in any halo scales as

$$p_N \propto \frac{[N + (3+n)/6\beta - 1 - 1/\beta]!}{N!}, \quad (53)$$

where $\nu \sim m^{(3+n)/6}$ and $\mu(m) \sim m^\beta$. As N becomes large, this behaves as a power law,

$$p_N \sim N^{-r}, \qquad r = 1 + \frac{1}{\beta} - \frac{(3+n)}{6\beta}. \quad (54)$$

For $n \approx -2$ and $\beta \lesssim 1$ the exponent is near $r = 2$, a good approximation to the distribution plotted in Fig. 1. For Sheth–Tormen the power is shifted by $2p(3+n)/6\beta$, or by about 0.1.

5.2 Resolved haloes

For small volumes we can no longer take haloes as point objects, but must take into account the distribution of objects within a halo. In the full halo model, the one-halo contribution to the k-point function ξ_k^{1h} for mass is a convolution of halo profiles (Ma & Fry 2000b),

$$\xi_k^{1h} = \frac{\int dm \, (dn/dm) \, m^k \int d^3r' u(y_1') \cdots u(y_k')}{\left[\int dm \, (dn/dm) \, m \int d^3r' \, u \, (y') \right]^k}, \quad (55)$$

where the position r' of the halo centre runs over all space, $y_i' = |r_i - r'|/r_s$, and the scaled halo profile $u(r)$ is normalized to unit integral. From equation (55), the volume-averaged correlation is then

$$\bar{\xi}_k^{1h} = \frac{\int dm \, (dn/dm) \, m^k \int d^3r' \, [F(r')]^k}{\left[\int dm \, (dn/dm) \, m \int d^3r' \, F \, (r') \right]^k}, \quad (56)$$

where $F(r')$ is the portion of the total volume of a halo centred at r' that lies within V,

$$F(r') = \int_0^R d^3r \, u \left(\frac{r - r'}{r_s} \right). \quad (57)$$

Note that the integrand is a function of r/r_s, and since the scale radius r_s depends on mass, the form factor F is in general also a function of halo mass. From equations (56) and (57) we can recover the point cluster model: if a volume is much larger than a halo size, $R \gg r_s$ for all haloes, then $F(r')$ is very small unless the halo itself is within V, in which case the integral then contains the entire halo contents. In this limit and with unit normalization, $F \to 1$ for r' in V and $F \to 0$ for r' outside V. Then, the integral over r' is just a factor of V, and we recover the point cluster model.

For resolved haloes in moments of discrete galaxy counts we consider first the second count moment $\bar{\xi}_2$. Let a halo contain N objects, and let N' be the number of these objects that are contained within V. Then $N' = \sum N_i$, where either $N_i = 1$ with probability p_i if object i is counted or $N_i = 0$ if object i is not, and the second moment is

$$\langle N'(N'-1) \rangle = \left\langle \sum_{i=1}^{N} N_i \left(\sum_{j=1}^{N} N_j - 1 \right) \right\rangle$$

$$= \left\langle \sum_{i \neq j} N_i N_j + \sum_{i=1}^{N} N_i^2 - \sum_{i=1}^{N} N_i \right\rangle. \tag{58}$$

But since N_i takes on the values 0 or 1, $N_i^2 = N_i$ and the last two terms cancel, leaving the sum only over distinct objects

$$\langle N'(N'-1) \rangle = \left\langle \sum_{i \neq j} N_i N_j \right\rangle = \langle N(N-1) \rangle p^2. \tag{59}$$

If object positions within a halo are uncorrelated, the probability p that an object within a given halo is located within the volume V is just the fraction F of the halo that is within V, form factor in equation (57), the same for all objects and independent of the halo occupation N,

$$\langle N'(N'-1) \rangle = \langle N(N-1) \rangle \langle F^2 \rangle. \tag{60}$$

This agrees with the usual practice, to distribute the average pair count $\langle N(N-1) \rangle$, weighted by the square of the halo profile form factor $\langle F^2 \rangle$,

$$\bar{\mu}_2 = \frac{\int dm\, (dn/dm)\, \langle N(N-1) \rangle\, \langle F^2 \rangle / \bar{n}_{\mathrm{h}}}{\left[\int dm\, (dn/dm)\, \langle N(m) \rangle / \bar{n}_{\mathrm{h}} \right]^2}, \tag{61}$$

where the volume-averaged form factor is

$$\langle F^k \rangle = \frac{1}{V} \int_0^\infty d^3 r' [F(\mathbf{r}')]^k. \tag{62}$$

In the position space formulation symmetry over all particles is manifestly maintained in the form-factor integrals, without need to introduce the approximation $W_{12} \approx W_1 W_2$. The form factor F does not appear in $\bar{N}$ in the denominator of equation (61), since, as can be easily seen by changing the order of integration, $\langle F \rangle = 1$. The calculation for a halo occupation distribution consisting of a central object plus $N_{\mathrm{s}} = N - 1$ satellites yields

$$\langle N'^{[2]} \rangle = \langle N_{\mathrm{s}}^{[2]} \rangle \langle F^2 \rangle + 2 \langle N_{\mathrm{s}} \rangle \langle F F_{\mathrm{c}} \rangle, \tag{63}$$

where $F_{\mathrm{c}} = 1$ for $r < R$ and vanishes otherwise. Extending to general k, we obtain

$$\langle N'^{[k]} \rangle = \langle N^{[k]} \rangle \langle F^k \rangle \tag{64}$$

with no central object, or

$$\langle N'^{[k]} \rangle = \langle N_{\mathrm{s}}^{[k]} \rangle \langle F^k \rangle + k \langle N_{\mathrm{s}}^{[k-1]} \rangle \langle F^{k-1} F_{\mathrm{c}} \rangle, \tag{65}$$

with a central object. The last term could contain a factor $\langle N_{\mathrm{c}} \rangle$ if this is not 1. The form-factor-corrected halo occupation moment is then

$$\bar{\mu}_k = \frac{\int dm\, (dn/dm)\, \langle N^{[k]}(m) \rangle\, \langle F^k \rangle / \bar{n}_{\mathrm{h}}}{\left[\int dm\, (dn/dm)\, \langle N(m) \rangle / \bar{n}_{\mathrm{h}} \right]^k}, \tag{66}$$

modified as in equation (65) for a central object.

For moments of dark matter mass, a reasonably good representation of the numerical results is obtained using the NFW profile, but for substructures this is not the case. The substructure profile was seen in Diemand, Moore & Stadel (2004) to follow roughly an
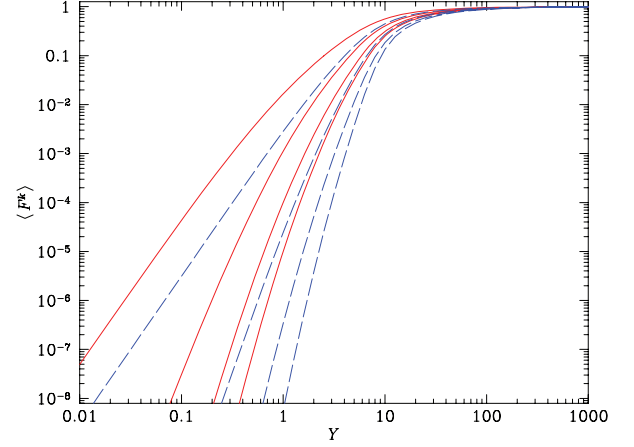

Figure 8. Volume-averaged form factor $\langle F^k \rangle$ for $k = 2$–5 (upper left to lower right), as a function of $Y = R/r_{\mathrm{s}}$. Solid lines show result for NFW profile; long-dashed lines show isothermal profile, both with $c = 10$.

isothermal profile, and we have studied using the isothermal sphere profile also. The measurements of Diemand et al. (2004) and our own do not provide enough statistics to infer a mass dependence of the concentration parameter, and so we use a constant value $c = 10$ that gives reasonable results on small scales. Fig. 8 shows the volume-averaged form factor for $k = 2$–5 for NFW haloes (solid lines) and for the isothermal sphere profile (long-dashed lines), both with $c = 10$. Curves are plotted as a function of $Y = R/r_{\mathrm{s}}$, where $r_{\mathrm{s}} = r_{200}/c$. As expected, the form factor goes to 1 at large scale and falls rapidly for small R, where only a small fraction of a halo is sampled. Note that $\langle F^k \rangle \leq \langle F^n \rangle$ if $k < n$. The integral converges to 1 on large scales, the point cluster regime, but falls rapidly for $Y < c$. In equation (66), for fixed R, this factor decreases rapidly for increasing mass.

Fig. 9 shows the form-factor-corrected, one-halo $S_k = \bar{\mu}_k / \bar{\mu}_2^{k-1}$, normalized by its value in the point-cluster limit, as a function of R, for $k = 3, 4$ and 5 (bottom to top; different orders k offset for clarity). On small scales, smaller than a few Mpc, this shows the effect of resolved haloes. The result depends both on halo profile and on
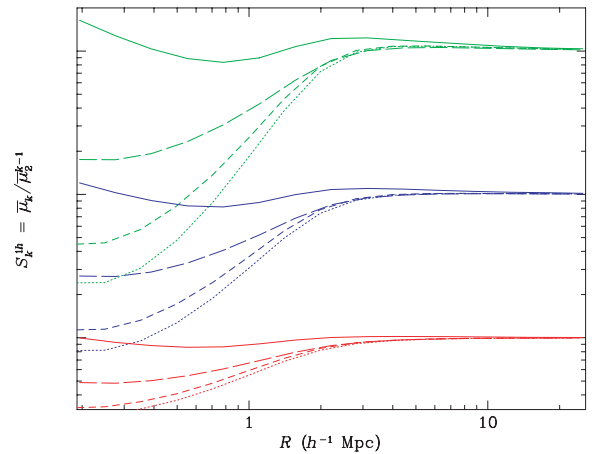

Figure 9. Form-factor-corrected one-halo S_k as a function of R, normalized to its point cluster value, for $k = 3, 4$ and 5 (bottom to top; different k offset for clarity). Solid lines show S_k for NFW profiles weighted by mass m^k; long-dashed lines show NFW profile weighted by number $N^{[k]}$; short-dashed lines show isothermal profile with $c = 10$ weighted by number and dotted lines show isothermal profile with $c = c(m)$.

the distribution function: solid lines show NFW haloes averaged over mass; long-dashed lines show the same haloes averaged over number; short-dashed lines show the isothermal profile with $c = 10$ and dotted lines show isothermal profiles with concentration $c(m)$ as for NFW. On large scales halo profile shape has no effect, but on small scales the differences for different profiles and weightings are substantial.

From the halo model can extract small-scale behaviours of the correlations $\bar{\xi}_k$, which can be different for galaxies and for mass. The concentration parameter plays a critical role in the result. For scale invariant spectra (cf. Davis & Peebles 1977) we expect $c(m) \sim M^{-\alpha}$, with $\alpha = (3 + n)/6$ (in Ma & Fry 2000a, this parameter is β). For Λ cold dark matter, over our relatively small range in mass we also take the concentration parameter to scale as a power of mass, $\alpha \approx 0.11$ or 0.12 (Bullock et al. 2001; Zhao et al. 2003), corresponding to an effective $n \approx -2.3$. As above, let the number of objects in a halo grow with mass as $\langle N^{[k]} \rangle \sim m^{k\beta}$ (for statistics of mass $\beta = 1$). Finally, let $\mathrm{d}n/\mathrm{d}m \sim \nu^{p'}/m^2$ as $m \to 0$, where $\nu \sim m^{(3+n)/6}$ and $p' = 1$ for PS and $p' = 1 - 2p = 0.4$ for ST (in Ma & Fry 2000a, this parameter is α). Then, ignoring the exponential factor in $\mathrm{d}n/\mathrm{d}m$ on small scales where ν is small and changing integration variable from m to $Y = R/r_s = cR/r_{200}$ in equation (66), we see that $\bar{\mu}_k$ scales as

$$\bar{\mu}_k \sim [R^{1/(\alpha+1/3)}]^{[k\beta+p'(3+n)/6-1]} \tag{67}$$

and the k-point function $\bar{\xi}_k = \bar{\mu}_k/\bar{N}_h^{k-1}$ scales as $R^{-\gamma_k}$, with

$$\gamma_k = \frac{3}{1+3\alpha}[3(k-1)\alpha + k(1-\beta)] - \frac{(3+n)p'}{2(1+3\alpha)} \tag{68}$$

$$= (k-1)\frac{3(5-2\beta+n)}{5+n} + \frac{6(1-\beta)}{5+n} - \frac{(3+n)p'}{5+n}, \tag{69}$$

independent of the shape of the halo profile. For $\beta = 1$ this is the same as the result obtained by Ma & Fry (2000a) (beware of a change of notation) for mass, and for $\beta = 1 - \epsilon$ is the result obtained by Scoccimarro et al. (2001) for galaxy number. This is of the hierarchical form only for $p' = 0$, which is not true for either of the PS or ST mass functions, and for $\beta = 1$. Departures from hierarchical scaling in the small-R behaviour of S_k grow with k,

$$S_k \sim R^{(k-2)\Delta\gamma}, \tag{70}$$

where

$$\Delta\gamma = \frac{(3+n)p' - 6(1-\beta)}{2(1+3\alpha)} = \frac{(3+n)p' - 6(1-\beta)}{5+n}. \tag{71}$$

Colombi et al. (1996) find in simulations of scale-free spectra that $S_k \propto \bar{\xi}_2^{(k-2)\delta}$, with $\delta = 0.045$. The halo model scalings in equations (69) and (71) predict this pattern with

$$\delta = \frac{p' - 6(1-\beta)/(3+n)}{3 - p' + 12(1-\beta)/(3+n)}, \tag{72}$$

which with $\beta = 1$ would require $p' = 0.13$.

The presence of ever higher powers of $\bar{\xi}_2$ in the reduced amplitude $S_k = \bar{\xi}_k/\bar{\xi}_2^{k-1}$ emphasizes any scaling defects in $\bar{\xi}_2$. An interesting alternative normalization is

$$S'_k = \frac{\bar{\xi}_k}{\bar{\xi}_{k-1}^{(k-1)/(k-2)}} = \frac{S_k}{S_{k-1}^{(k-1)/(k-2)}}. \tag{73}$$

Departures from scaling in S'_k decrease with k for $k \geq 3$, as

$$S'_k \sim R^{\Delta\gamma/(k-2)} \tag{74}$$

for the same $\Delta\gamma$ given in equation (71).

5.3 Multiple-halo terms

Terms that involve objects in multiple haloes also depend on correlations among haloes. In the perturbative regime, halo correlations have bias factors that are functions of the halo masses, and higher order correlation functions also involve higher order bias parameters (Fry & Gaztañaga 1993); for instance, the halo three-point function is

$$\xi_{3,h} = b(m_1)b(m_2)b(m_3)\,\xi_{3,\rho}(r_{12}, r_{13}, r_{23})$$
$$+ b_2\,[\xi_{2,\rho}(r_{12})\xi_{2,\rho}(r_{13}) + \text{cyc. (123)}], \tag{75}$$

where the ξ_ρ are correlation statistics for the underlying (primordial) density distribution. As a function of mass, the linear bias factor found for PS by Mo, Jing & White (1996, 1997) and adapted for the ST halo mass function (ST; Casas-Miranda, Mo & Boerner 2003) is

$$b = 1 + \frac{q\nu^2 - 1}{\delta_c} + \frac{2p}{\delta_c}\frac{1}{[1 + (q\nu^2)^p]}, \tag{76}$$

with further refinements for small mass suggested by Jing (1999). Higher order functions also require higher order bias parameters (Mo et al. 1997; Scoccimarro et al. 2001),

$$b_2 = \frac{8}{21\delta_c}\left\{q\nu^2 - 1 + \frac{2p}{[1 + (q\nu^2)^p]}\right\}$$
$$+ \frac{1}{\delta_c^2}\left\{q^2\nu^4 - 3q\nu^2 + \frac{2p(q\nu^2 + 2p - 1)}{[1 + (q\nu^2)^p]}\right\}, \tag{77}$$

etc. Higher order bias terms b_3, etc., vanish when integrated over the full halo mass function. Even with a low-mass cut-off or with different mass or number weightings we expect that they remain generally small, and so we will drop them from now on (but see Angulo, Baugh & Lacey 2008).

We exhibit in detail the k-halo and two-halo contributions to $\bar{\xi}_k$ in the full halo model. The k-halo contribution to $\bar{\xi}_k$ is

$$\bar{N}^k \xi_k^{kh} = \prod_{i=1}^{k} \int \mathrm{d}m_i \frac{\mathrm{d}n}{\mathrm{d}m_i} \langle N(m_i) \rangle$$
$$\times \int \mathrm{d}^3r'_1\, u(y'_1) \cdots \mathrm{d}^3r'_k\, u(y'_k)\, \xi_{k,h}(\mathbf{r}'_1, \ldots, \mathbf{r}'_k), \tag{78}$$

where $\bar{N}$ is as given in equation (42). Ignoring non-linear bias terms, so that in terms of the underlying density correlation $\xi_{k,\rho}$ the halo correlation function is $\xi_{k,h} = b(m_1) \cdots b(m_k)\, \xi_{k,\rho}$, the volume-averaged correlation becomes

$$\bar{N}^k \bar{\xi}_k^{kh} = \prod_{i=1}^{k} \int \mathrm{d}m_i \frac{\mathrm{d}n}{\mathrm{d}m_i} b(m_i) \langle N(m_i) \rangle$$
$$\times \int \mathrm{d}^3r'_1\, F(r'_1) \cdots \mathrm{d}^3r'_k\, F(r'_k)\, \xi_{k,\rho}(\mathbf{r}'_1, \ldots, \mathbf{r}'_k). \tag{79}$$

In the point cluster limit on large scales, for which $F = 1$ for $\mathbf{r}'$ in V and $F = 0$ for $\mathbf{r}'$ outside V, this gives

$$\bar{\xi}_{k,h}^{kh} = \bar{b}^k \bar{\xi}_{k,\rho} = \frac{\bar{b}^k}{\bar{b}_h^k} \bar{\xi}_{k,h}, \tag{80}$$

with an occupation-number weighted bias factor,

$$\bar{b} = \frac{\int \mathrm{d}m\,(\mathrm{d}n/\mathrm{d}m)\,\langle N(m) \rangle\, b(m)}{\int \mathrm{d}m\,(\mathrm{d}n/\mathrm{d}m)\,\langle N(m) \rangle}. \tag{81}$$

The halo correlation function $\bar{\xi}_{k,h}$ is $\bar{\xi}_{k,h} = \bar{b}_h^k \bar{\xi}_{k,\rho}$, with a bias factor weighted only by the halo mass distribution,

$$\bar{b}_h = \frac{\int \mathrm{d}m\,(\mathrm{d}n/\mathrm{d}m)\,b(m)}{\int \mathrm{d}m\,(\mathrm{d}n/\mathrm{d}m)}. \tag{82}$$

Factors of mass or number weight greater contributions at higher masses, where $b(m)$ takes on larger values, so in general $\bar{b} > \bar{b}_{\mathrm{h}}$; galaxies are more strongly correlated than haloes on large scales, though only by a small amount. Ratios of integrals $\bar{b}/\bar{b}_{\mathrm{h}}$ over the Sheth–Tormen mass function with $\langle N \rangle \propto m$ for mass and $\langle N \rangle \propto m^\beta$ with $\beta = 0.8$ for number are listed in Table 2.

Similarly, we can write intermediate terms. The two-halo contribution to $\bar{\xi}_k$ is a sum of terms of the form

$$\bar{N}^k \bar{\xi}_k^{2\mathrm{h}} = \frac{s\,k!}{k_1!\,k_2!} \int \mathrm{d}m_1 \frac{\mathrm{d}n}{\mathrm{d}m_1}\, \mathrm{d}m_2 \frac{\mathrm{d}n}{\mathrm{d}m_2} \left\langle N_1^{[k_1]} \right\rangle \left\langle N_2^{[k_2]} \right\rangle$$
$$\times \int \mathrm{d}^3 r_1'\, \mathrm{d}^3 r_2'\, [F(r_1')]^{k_1} [F(r_2')]^{k_2} b(m_1) b(m_2)\, \xi_2(r_{12}'),$$
(83)

where $k = k_1 + k_2$. (If $k_1 = k_2$ there is an additional symmetry factor of $s = 1/2$ because the partition and its complement are identical; the generating function gives all combinatoric factors automatically.) On large scales, where the halo size is insignificant and the form factors take the value $F = 1$ over essentially the entire volume V, the full two-halo term is thus the sum over partitions

$$\bar{\xi}_k^{2\mathrm{h}} = \frac{sk!}{k_1!\,k_2!} \frac{\bar{b}_{k_1}}{\bar{b}_{\mathrm{h}}} \frac{\bar{b}_{k_2}}{\bar{b}_{\mathrm{h}}} \frac{\bar{\mu}_{k_1} \bar{\mu}_{k_2}\, \bar{\xi}_{2,\mathrm{h}}}{\bar{N}_{\mathrm{h}}^{k-2}},$$
(84)

where $\bar{b}_k$ is weighted by $\langle N^{[k]} \rangle$,

$$\bar{b}_k = \frac{\int \mathrm{d}m\, (\mathrm{d}n/\mathrm{d}m)\, \langle N^{[k]}(m) \rangle \langle F^k \rangle b(m)}{\int \mathrm{d}m\, (\mathrm{d}n/\mathrm{d}m)\, \langle N^{[k]} \rangle \langle F^k \rangle}.$$
(85)

For moments of mass, the factors $\langle N^{[k]}(m) \rangle$ become m^k. Weighted by different factors of number or mass, the bias parameters $\bar{b}_k$ will in general be different from $\bar{b} = \bar{b}_1$ defined in equation (81); the lower mass limit for the integral also increases for higher order moments. On small scales, where haloes are resolved, the halo size, and thus the factor $F(r')$, depends also on halo mass: the mass and position integrals cannot be factored or simplified. However, since $F \leq 1$, the expression in equation (84) is an upper limit to the two-halo contribution, and even without the form factors the two-halo contribution is dominated by the one-halo term given in equation (56) as $R \to 0$. Extension to other intermediate orders follows similar lines.

6 DISCUSSION

We have studied the behaviour of cell count moments, including the variance $\bar{\xi}_2$ and the hierarchal amplitudes S_k for $k = 3$, 4 and 5, in the context of the halo model, and we have compared the model with results of numerical simulations for statistics mass and of galaxy (substructure) number counts identified in the same simulation. Expressions (29)–(32) constitute the halo model predictions for the two-, three-, four- and five-point functions; a composition of generating functions for the halo number and halo occupancy distributions, as presented in equation (33), produces automatically the halo model result at general order, including all terms and combinatoric factors. The naive, point-cluster form of the model with identical haloes is easily generalized to include averages over a distribution of halo masses and over positions within resolved haloes. The general form of the naive point cluster model results continues to hold, with the addition of a modest bias, a factor of 2 or less, on large scales, and form factors that reflect shapes of resolved haloes on small scales. With these components, the halo model is able to reproduce in quantitative detail statistical moments for mass and for substructure samples whose densities vary by a factor of 100.

On scales greater than of the order of a few Mpc, theoretical predictions are well represented in the point cluster version of the halo model. On the largest scales, the point cluster model reproduces the results of perturbation theory with bias (Bernardeau et al. 2002). On intermediate scales, spanning $\bar{N}\bar{\xi} \lesssim 1$ where single-halo terms begin to dominate but haloes are still unresolved, halo model results are still robust, independent of details such as halo profile, asphericity and concentration parameter, but different from perturbation theory: the variance $\bar{\xi}_2 = \bar{\mu}_2 / \bar{N}_{\mathrm{h}}^2$ steepens as a function of r, approaching r^{-3}, an effect seen in scaling studies (Hamilton et al. 1991; Peacock & Dodds 1996); and the amplitudes S_k are constant, as in the plateau seen in scale-free models by Colombi et al. (1996), at values determined by occupation probabilities. The halo model with Press–Schechter or Sheth–Tormen mass function allows us to compute from first principles values for the hierarchical amplitudes S_k for scale-invariant models with power spectrum $P \sim k^n$. As shown in Fig. 7, the halo model predictions are sensitive to the mass function and to mass cutoffs. For scale-free models with initial spectrum $P(k) \sim k^n$, the halo model reproduces the general trends of $S_k(n)$. Disagreements for more negative n are probably an indication of the difficulty of simulating these spectra.

The largest halo has $r_{\mathrm{s}} \approx 500\,h^{-1}$ kpc; on scales smaller than this, we must include the effects of finite halo size. Resolved haloes introduce scale-dependent form factors in the $\bar{\mu}_{k,i}(R)$, as in Section 4. Analysis of resolved haloes is made substantially more efficient by analytic expressions for the form factors, contained in Appendix C. Small-scale results suggest that the profile shape is different for mass and for substructures. In our limited efforts we have not found a profile shape that allows us to fit the shape of S_k on all scales in the resolved halo regime. For that matter, we do not really know that a universal profile shape applies for the distribution of galaxies within haloes of different size. A possible explanation is that tidal disruption leads to no universal profile that applies on all scales, or the halo model picture itself may be oversimplistic. Nevertheless, on large scales our simulation and model results seem to have the potential to agree with observations (Ross, Brunner & Myers 2006).

As observations become more and more precise, so it is increasingly important to be able to model clustering statistics with precision. This appears to be possible for mass on both large and small scales. On large scales, perturbation theory (biased linear theory) is accurate to better than 1 per cent. On small scales, where statistics are dominated by tightly bound, high-density collapsed haloes, using published forms for the mass function $f(m)$ and the concentration parameter $c(m)$ with no attempt to optimize, the halo model reproduces the variance for our simulation again to within a few per cent. This is suggestive but not in itself a proof of the halo model; history has shown that there may be many constructs that lead to the same two-point function; thus, it is a non-trivial result that the halo model also reproduces with accuracy the higher order correlation functions on small and large scales as well. There are somewhat larger deviations on intermediate scales, where the halo model predictions are too large by 5–10 per cent, in a direction that is only made worse by including higher order perturbative corrections. This is a regime where the halo model seems to be least likely to be valid, where there is a significant amount of inhomogeneously clustered mass not contained in spherical haloes; another interesting possibility in this regime is renormalized perturbation theory (Crocce & Scoccimarro 2006). The halo model predictions also match very well number count statistics on both large and intermediate scales, the point cluster regime, across all the different subcatalogues with different mass thresholds. This is perhaps not a surprise, since there is no 'background' population, objects in haloes account for all the objects there are. However, such precision is not reached on small scales. With a small number of haloes, we do not know the profile

shape, although it seems that the NFW profile does not work, and we do not know how the halo radius or concentration parameter depends on mass. This may be the result of using substructures instead of galaxies in a full hydrodynamic simulation; substructures in high-density regions may be tidally disrupted (Weinberg et al. 2008). We present results using an isothermal profile with fixed $c = 10$, but this is at best only a first approximation.

Halo model statistics computed over mass and number distributions taken from the simulation work well. It is in principle possible to compute correlations from first principles, starting with a primordial power spectrum, using the Sheth–Tormen halo mass function and a prescription such as a Poisson satellite number. Application to scale-free simulations with initial spectrum $P \sim k^n$ gives plausible results for $S_k(n)$, at least for n not too negative, once taking into account finite simulation resolution. In practice, the predicted relative bias factors $\bar{b}_g/\bar{b}_h$ do not quite match the numerical results, but this is probably due to finite volume effects. In particular, the halo five-point function is barely detected.

In the end, on small scales there are substantial differences between the discrete statistics of number counts and the continuous statistics of mass. The distribution function of halo occupation number has a behaviour different from that of the distribution of halo mass, and factorial moments of discrete counts behave differently than moments of mass, even if the mean occupation number itself were a faithful tracer of total mass, all of which contribute to differences in S_k, both in value and in shape as a function of scale, to the extent that it is not clear that the concept of bias between galaxy and mass statistics, even a non-linear bias, is a useful concept.

It may sometimes seem that with a halo profile shape, mass function, concentration parameter and asphericity all to be specified, the halo model is infinitely adjustable. However, on intermediate and large scales much of this freedom disappears, and the model depends only on the compounding of statistics. In the halo model calculation, we see that the overall size of the correlation function $\bar{\xi}_k$ or the amplitude S_k is determined by moments $\bar{\mu}_k = \langle m^k \rangle$ of mass or factorial moments $\bar{\mu}_k = \langle N^{[k]} \rangle$ of halo occupation number, while details of shape on small scales provide information on the halo profile, $\langle F^k \rangle$. That the model can reproduce in detail the measured S_k for $k = 3$–5, simultaneously for both mass and number, and can handle probabilities as well as moments, is a non-trivial success.

REFERENCES

Angulo R. E., Baugh C. M., Lacey C. G., 2008, MNRAS, 387, 921
Aubert D., Pichon C., Colombi S., 2004, MNRAS, 352, 376
Berlind A. A., Weinberg D. H., 2002, ApJ, 575, 587
Berlind A. A. et al., 2003, ApJ, 593, 1
Bernardeau F., 1992, ApJ, 392, 1
Bernardeau F., Colombi S., Gaztañaga E., Scoccimarro R., 2002, Phys. Rep., 367, 1
Blaizot J. et al., 2006, MNRAS, 369, 1009
Bullock J. S., Kolatt T. S., Sigad Y., Somerville R. S., Kravtsov A. V., Klypin A. A., Primack J. R., Dekel A., 2001, MNRAS, 321, 559
Casas-Miranda R., Mo H. J., Boerner G., 2003, MNRAS, 339, 872
Colombi S., Bouchet F. R., Hernquist L., 1996, ApJ, 465, 14
Colombi S., Chodorowski M. J., Teyssier R., 2007, MNRAS, 375, 348 (CCT)
Cooray A., Sheth R., 2002, Phys. Rep., 372, 1
Cowpertwait P. S. P., 1994, R. Soc. Lond. Proc. Ser. A, 447, 23
Crocce M., Scoccimarro R., 2006, Phys. Rev. D., 73, 063519
Davis M., Peebles P. J. E., 1977, ApJS, 34, 425
Diemand J., Moore B., Stadel J., 2004, MNRAS, 352, 535
Evin G., Favre A.-C., 2008, Water Resour. Res., 44, W03433
Finkelstein J., 1988, Phys. Rev. D, 37, 2446
Fry J. N., 1984, ApJ, 279, 499
Fry J. N., 1985, ApJ, 289, 10
Fry J. N., Gaztañaga E., 1993, ApJ, 413, 447
Hamilton A. J. S., Kumar P., Lu E., Matthews A., 1991, ApJ, 374, L1
Hegyi S., 1994, Phys. Lett. B., 327, 171
Hockney R. W., Eastwood J. W., 1981, Computer Simulation Using Particles. McGraw Hill, New York
Jain B., Bertschinger E., 1998, ApJ, 509, 517
Jing Y. P., 1999, ApJ, 515, L45
Juszkiewicz R., Bouchet F. R., Colombi S., 1993, ApJ, 412, L9
Kravtsov A. V., Berlind A. A., Wechsler R. H., Klypin A. A., Gottlöber S., Allgood B., Primack J. R., 2004, ApJ, 609, 35
Ma C.-P., Fry J. N., 2000a, ApJ, 538, L107
Ma C.-P., Fry J. N., 2000b, ApJ, 543, 503
McClelland J., Silk J., 1977, ApJ, 217, 331
Mo H. J., Jing Y. P., White S. D. M., 1996, MNRAS, 282, 1096
Mo H. J., Jing Y. P., White S. D. M., 1997, MNRAS, 284, 189
Monaghan J. J., 1992, ARA&A, 30, 543
Moore B., Quinn T., Governato F., Stadel J., Lake G., 1999, MNRAS, 310, 1147
Navarro J. F., Frenk C. S., White S. D. M., 1997, ApJ, 490, 493
Navarro J. F. et al., 2004, MNRAS, 349, 1039
Neyman J., Scott E. L., 1952, ApJ, 116, 144
Peacock J. A., Dodds S. J., 1996, MNRAS, 280, L19
Peacock J. A., Smith R. E., 2000, MNRAS, 318, 1144
Peebles P. J. E., 1980, The Large-Scale Structure of the Universe. Princeton Univ. Press, Princeton
Press W. H., Schechter P., 1974, ApJ, 187, 425 (PS)
Rodriguez Iturbe I., Cox D. R., Isham V., 1987, R. Soc. Lond. Proc. Ser. A, 410, 269
Ross A. J., Brunner R. J., Myers A. D., 2006, ApJ, 649, 48
Saslaw W. C., 1989, ApJ, 341, 588
Saslaw W. C., Hamilton A. J. S., 1984, ApJ, 276, 13
Scherrer R. J., Bertschinger E., 1991, ApJ, 381, 349
Scoccimarro R., Frieman J. A., 1999, ApJ, 520, 35
Scoccimarro R., Sheth R. K., Hui L., Jain B., 2001, ApJ, 546, 20
Seljak U., 2000, MNRAS, 318, 203
Sheth R. K., 1995a, MNRAS, 274, 213
Sheth R. K., 1995b, MNRAS, 276, 796
Sheth R. K., 1996, MNRAS, 281, 1124
Sheth R. K., Saslaw W. C., 1994, ApJ, 437, 35
Sheth R. K., Tormen G., 1999, MNRAS, 308, 119 (ST)
Smith R. E. et al., 2003, MNRAS, 341, 1311
Soneira R. M., Peebles P. J. E., 1977, ApJ, 211, 1
Szapudi I., 1998, ApJ, 497, 16
Szapudi I., Szalay A. S., 1993, ApJ, 408, 43
Szapudi I., Quinn T., Stadel J., Lake G., 1999, ApJ, 517, 54
Tchikilev O. G., 1999, Phys. Rev. D, 59, 94008
Teyssier R., 2002, A&A, 385, 337
Weinberg D. H., Colombi S., Davé R., Katz N., 2008, ApJ, 678, 6
Zhao D. H., Jing Y. P., Mo H. J., Börner G., 2003, ApJ, 597, L9
Zheng Z., Weinberg D. H., 2007, ApJ, 659, 1

Zheng Z. et al., 2005, ApJ, 633, 791

Zheng Z., Coil A. L., Zehavi I., 2007, ApJ, 667, 760

Zheng Z., Zehavi I., Eisenstein D. J., Weinberg D. H., Jing Y. P., 2009, ApJ, 707, 554

APPENDIX A: EMPTY HALOES

We show in this Appendix that for every composite distribution P_N that includes empty haloes with a non-zero probability $q_0 \neq 0$, there is another with $q'_0 = 0$ that produces the same P_N. Thus, excluding (or including) empty haloes does not impose a physical restriction on the resulting occupation distribution P_N.

Suppose we start with a distribution with $q_0 \neq 0$. Then, the total count probabilities will include contributions from many clusters with no occupancy,

$$P_0 = p_0 + p_1 q_0 + p_2 q_k^2 + p_3 q_0^3 + \cdots \qquad (A1)$$

$$P_1 = p_1 q_1 + 2 p_2 q_1 q_0 + 3 p_3 q_1 q_0^2 + \cdots \qquad (A2)$$

$$P_2 = p_1 q_2 + p_2 \left(q_1^2 + 2 q_2 q_0\right) + p_3 \left(3 q_2 q_0^2 + 3 q_1^2 q_0\right) + \cdots \qquad (A3)$$

$$P_3 = p_1 q_3 + p_2 \left(2 q_1 q_2 + 2 q_3 q_0\right)$$
$$+ p_3 \left(q_1^3 + 6 q_1 q_2 q_0 + 3 q_3 q_0^2\right) + \cdots. \qquad (A4)$$

We can easily create an occupancy distribution with no empty haloes while maintaining the same relative probabilities by defining a new set of probabilities q'_n such that $q'_0 = 0$ and $q'_n = q_n/(1 - q_0)$ for $n > 0$. This distribution has the generating function

$$g'_i(z) = \frac{g_i(z) - q_0}{1 - q_0}. \qquad (A5)$$

Note that since $g_i(0) = q_0$, this gives $g'_i(0) = 0$, and $g'_i(1) = g_i(1) = 1$.

We can then modify the halo occupation number probability p'_n in what turns out to be a sensible way to produce in the end the same P_N. With $q'_0 = 0$ we must have $P_0 = p'_0$, so we take

$$p'_0 = \sum_{n=0}^{\infty} p_n q_0^n = g_h(q_0). \qquad (A6)$$

Next, to have $P_1 = p'_1 q'_1$,

$$p'_1 q'_1 = \frac{p'_1 q_1}{1 - q_0} = \sum_{n=0}^{\infty} n p_n q_1 q_0^{n-1} = q_1 \left. \frac{dg_h(z)}{dz} \right|_{z=q_0}, \qquad (A7)$$

we take $p'_1 = (1 - q_0)(dg_h/dz)|_{q_0}$. Similarly, to have

$$P_2 = p'_1 q'_2 + p'_2 q'^2_1$$

$$= q_2 \sum n p_n q_0^{n-1} + q_1^2 \frac{1}{2} \sum n(n-1) p_n q_0^{n-1}, \qquad (A8)$$

we take $p'_2 = \frac{1}{2}(1 - q_0)^2 (d^2 g_h/dz^2)|_{q_0}$. These p'_n follow from the generating function

$$g'_h(z) = g_h[(1 - q_0)z + q_0]. \qquad (A9)$$

The coefficient of each term in the expansion is a sum of products of positive numbers with positive coefficients, and so $p'_n \geq 0$; and $g'_h(1) = g_h(1 - q_0 + q_0) = 1$, so that each term must satisfy $p'_n \leq 1$ and the distribution is properly normalized. The composition of these two modified distributions then gives

$$G'(z) = g'_h[g'_i(z)] = g_h[(1 - q_0) g'_i(z) + q_0] = g_h[g_i(z)], \qquad (A10)$$

and so the same P_N, as desired.

For the case of a Poisson cluster number distribution, Finkelstein (1988) shows that the revised p'_n again are a Poisson distribution with mean $\bar{N}' = \bar{N}(1 - q_0)$. The general case has essentially the same interpretation. The continuum (discreteness corrected) moments, generated by $M(t) = G(1 + t)$, follow from

$$M'_h(t) = G'(1 + t) = G[(1 - q_0)(1 + t) + q_0]$$
$$= G[1 + (1 - q_0)t] = M[(1 - q_0)t]. \qquad (A11)$$

Thus, continuum moments are scaled by a factor $(1 - q_0)^n$ which absorbed in the mean $\bar{N}'_i = \bar{N}_i(1 - q_0)$, leave the correlations $\bar{\mu}_n$ unchanged: the q'_k are a discrete realization of the same underlying number density field. In a sense, this is the equivalent of including an unclustered background, as in equation (36).

In general, q_0 can be mapped to any value $0 < \alpha < 1$ by the transformations

$$g'_i(z) = \frac{g_i(z) - \alpha}{1 - \alpha}, \qquad g'_h(z) = g_h[(1 - \alpha)z + \alpha], \qquad (A12)$$

and it remains true that the generating function of total count probabilities is unchanged, $G(z) = g'_h[g'_i(z)] = g_h[g_i(z)]$.

APPENDIX B: ALGORITHMS FOR COMPUTING THE COUNT-IN-CELL DISTRIBUTION FUNCTION

In this Appendix we detail how the count-in-cell distribution function $P_N(\ell)$ is estimated in these samples. There exist many efficient ways to measure this function in cubical cells (e.g. Szapudi 1998; Szapudi et al. 1999; Blaizot et al. 2006). The problem is, however, more intricate for spherical cells of radius ℓ, which we prefer to use in this paper, since the analytical calculations are much easier to derive for these latter. Although it is rather usual and fair to approximate spherical cells with cubical cells of same volume with a small form factor correction (e.g. Szapudi 1998, and references therein), we prefer here to avoid this approximation. Then, the two most common ways of measuring function $P_N(\ell)$ for spherical cells are as follows.

(i) *The FFT method*: it consists of assigning the particles to a grid of size N_{grid} using e.g. nearest grid point or cloud-in-cell interpolation (e.g. Hockney & Eastwood 1981), Fast Fourier Transform (FFT) the corresponding density distribution, multiply the result by the Fourier transform of the top hat filter in Fourier space and then Fourier transform back to estimate function $P_N(\ell)$. Obviously, the FFT method is valid only if the cell size is much larger than the size of a mesh element.

(ii) *The direct assignment method*: it consists of creating a list of candidate cells positioned on a regular pattern of size N_{grid}, then on scanning the list of particles and assigning them to each cell when relevant to augment the corresponding count. This method does not suffer the defects of the FFT, so can be used even for very small scales, but can become prohibitive at large scales, when the network of cells starts to significantly self-overlap (i.e. a particle is assigned to a large number of cells).

Naturally, a good choice consists of using the direct assignment method at small scales and the FFT method at large scales. However, the very large number of particles, 512^3, in our full RAMSES dark matter called for an additional algorithmic improvement, valid at intermediate scales. Our implementation, COUNTKD, is a code based on a decomposition of space using standard oct-tree technique, similarly as in Szapudi et al. (1999), but for spherical cells. The oct-tree decomposition allows one to approximate a spherical cell with a

Table B1. Parameters used to perform the count-in-cells measurements. The first line gives the inverse scale in units of the simulation box size L_{box}/ℓ; the smallest and the largest scales, $L_{box}/\ell = 1024$ and $L_{box}/\ell = 8$, correspond to $\ell = 0.2\,h^{-1}$ Mpc and $\ell = 25\,h^{-1}$ Mpc, respectively. The second line gives the size of the grid of sampling cells, N_{grid}, used to perform the measurements at a given ℓ for the full dark matter sample, RAMSES; $N_{grid} = 2048$ means that 2048^3 cells were used, corresponding to a minimum possible value of P_N of the order of 1.16×10^{-10}. The third line identifies the count-in-cell measurement method used for each scale under consideration, T for oct-tree walk, F for FFT and D for direct assignment. The fourth and fifth lines give N_{grid} and the method for all the other samples.

L_{box}/ℓ	1024	$512\sqrt{2}$	512	$256\sqrt{2}$	256	$128\sqrt{2}$	128	$64\sqrt{2}$	64	$32\sqrt{2}$	32	$16\sqrt{2}$	16	$8\sqrt{2}$	8
RAMSES															
N_{grid}	2048	2048	2048	2048	2048	2048	1024	1024	1024	1024	512	512	512	512	512
Method	T	T	T	T	T	T	T	T	T	T	T	T	F	F	F
Others															
N_{grid}	1024	1024	1024	1024	1024	1024	1024	1024	1024	1024	512	512	512	512	512
Method	D	D	D	D	D	D	D	D	D	D	D	D	D	D	D

coverage of cubes of varying size; this latter decreasing (by factors of 2) when approaching the cell boundary. At some point, when the maximum allowed level of refinement is reached (or when there is only one particle per oct-tree cell), the position of particles themselves is used to decide if they belong to the cell in consideration or not. Obviously, this method is efficient only if there are sufficiently many particles per cell, otherwise it is faster to perform direct assignment as explained above. For this work, we did not bother to find the optimal compromise between direct assignment, oct-tree walk and FFT method and performed the measurements as described in Table B1. The main goal was simply to reach a reasonable level of accuracy to sample correctly the large N tails of function $P_N(\ell)$ in a reasonable amount of CPU time while avoiding as much as possible the FFT method which is sensitive to the pixelization of the data.

APPENDIX C: FORM-FACTOR INTEGRALS

In this Appendix we present analytic expressions for the form factors $F(x; y, c)$, the fraction of a halo with concentration parameter c and centre at $r/r_s = x$ that is contained within a spherical volume of radius $R/r_s = y$. First, note that the volume $\mathcal{V}$ of the intersection of two spheres of radii a and b whose centres are separated by distance d is

$$\mathcal{V}(a, b, d) = \begin{cases} I(a, b, d), & |a - b| \leq d \leq a + b, \\ 0, & d > a + b, \\ \frac{4\pi}{3} \min(a^3, b^3), & d \leq |a - b|, \end{cases} \quad (C1)$$

where the shared volume $I(a, b, d)$ of spheres that partially overlap is

$$I(a, b, d) \equiv \frac{\pi}{d} \left[\frac{1}{12} d^4 - \frac{1}{2} d^2 (a^2 + b^2) \right.$$
$$\left. + \frac{2}{3} d(a^3 + b^3) - \frac{1}{4}(a^2 - b^2)^2 \right]. \quad (C2)$$

Next, note that a decreasing profile $\rho(r)$ can be modelled as a sum of step functions, truncated at an outer radius r_{max}. This means that the profile is composed of an ensemble of spheres of decreasing densities ρ_i and increasing radii r_i, $i = 0, \ldots, N$, with $r_0 = 0$, $r_N = r_{max}$. Then, for $\rho(r) = \rho_i$ for $r_{i-1} < r \leq r_i$, we can write

$$\rho(r) = \rho_N - \sum_{r_i > r} \Delta\rho_i, \quad \Delta\rho_i \equiv \rho_i - \rho_{i-1}. \quad (C3)$$

Now, let us compute the mass contained within radius R of the origin for a halo centred at a distance d,

$$M(d, R) = \int_{r < R} \mathrm{d}^3 r \, \rho(\boldsymbol{d} + \boldsymbol{r}). \quad (C4)$$

From equation (C3), the calculation reduces to the sum of intersections of spheres with appropriate weights,

$$M(d, R) = \rho(r_{max}) \mathcal{V}(R, r_{max}, d) - \sum_i \mathcal{V}(r_i, R, d)\Delta\rho_i. \quad (C5)$$

In the continuous limit, we obtain the final expression

$$M(d, R) = \rho(r_{max}) \mathcal{V}(R, r_{max}, d)$$
$$- \int_{|R-r| < d < r+R}^{r < r_{max}} I(r, R, d) \frac{\mathrm{d}\rho}{\mathrm{d}r} \, \mathrm{d}r$$
$$- \int_{d < |r-R|}^{r < r_{max}} \frac{4\pi}{3} \min(R^3, r^3) \frac{\mathrm{d}\rho}{\mathrm{d}r} \, \mathrm{d}r. \quad (C6)$$

We apply this in particular to the NFW and isothermal sphere profiles.

C1 Convolution of the NFW profile

The truncated NFW profile writes, in scaled units

$$\rho_{NFW}(r) = \begin{cases} \frac{1}{r(1+r)^2}, & r \leq c, \\ 0, & r > c. \end{cases} \quad (C7)$$

The calculation of the integral gives

$$M_{NFW}(x) = -\left\{ I(r, y, x)\rho(r) - \frac{2\pi(x+1)}{x} \ln(1 + r) \right.$$
$$\left. + \frac{\pi r}{x} - \frac{\pi r}{x} \left[\frac{y^2 - (x+1)^2}{1 + r} \right] \right\}_{r=r_-}^{r=r_+}$$
$$- \left\{ \frac{4}{3}\pi r^3 \rho(r) - 4\pi \left[\frac{1}{r+1} + \ln(r+1) \right] \right\}_{r=0}^{r=r_1}$$
$$- \left\{ \frac{4}{3}\pi y^3 \rho(r) \right\}_{r=r_-}^{r=c} + \rho(c)\mathcal{V}(c, y, x), \quad (C8)$$

where $\rho = \rho_{NFW}$, $x = d/r_s$, $Y = R/r_s$, $c = r_{max}/r_s$ and

$$r_+ = \min(c, x + y), \quad (C9)$$

$$r_- = \min(c, |x - y|), \quad (C10)$$

$$r_1 = \min[c, \max(y - x), 0)]. \tag{C11}$$

Evaluated for $y > c$ and $x = 0$ this gives the total mass,

$$M = 4\pi \frac{[(1 + c) \ln(1 + c) - c]}{(1 + c)}, \tag{C12}$$

and the normalized NFW form factor is then

$$F_{\mathrm{NFW}}(x, Y, c) = \frac{M_{\mathrm{NFW}}(x; Y, c)}{4\pi[(1 + c) \ln(1 + c) - c]/(1 + c)}. \tag{C13}$$

C2 Convolution of the isothermal profile

The isothermal profile writes, in scaled units

$$\rho_{\mathrm{ISO}}(r) = \begin{cases} \frac{1}{1 + r^2}, & r \leq c, \\ 0, & r > c. \end{cases} \tag{C14}$$

The calculation of the integral gives

$$
\begin{aligned}
M_{\mathrm{ISO}}(x) = -&\left\{ I(r, x, d)\rho(r) - 2\pi(r - \arctan r) \right. \\
&\left. + \frac{\pi}{2x} \left[(x^2 - y^2 - 1) \log(1 + r^2) + r^2 \right] \right\}_{r=r_-}^{r=r_+} \\
&- \left\{ \frac{4\pi}{3} r^3 \rho(r) - 4\pi(r - \arctan r) \right\}_{r=0}^{r=r_1} \\
&- \left\{ \frac{4}{3} \pi y^3 \rho(r) \right\}_{r=r_-}^{r=c} + \rho(c) \mathcal{V}(c, y, x),
\end{aligned} \tag{C15}
$$

where $\rho = \rho_{\mathrm{ISO}}$ and r_+, r_- and r_1 are as in equations (C9)–(C11). Evaluated for $y > c$ and $x = 0$ this gives the total mass,

$$M = 4\pi(c - \arctan c), \tag{C16}$$

and the normalized form factor for the isothermal profile is

$$F_{\mathrm{ISO}}(x, Y, c) = \frac{M_{\mathrm{ISO}}(x; Y, c)}{4\pi(c - \arctan c)}. \tag{C17}$$

This paper has been typeset from a TeX/LaTeX file prepared by the author.